AUT Journal of Electrical Engineering
10.22060/EEJ.2026.24986.5808

Design and Implementation of an Improved Dynamic Response Flying Capacitor Boost Converter for Smart Grid Systems Using a Model Predictive Controller

Kudiyarasan Swamynathan[1,*], S. Kamatchi[2]

[1]PhD., DGM (Electrical), Renewable Energy Power Plants, Neyveli Lignite Corporation India Limited (NLCIL), Neyveli, Tamilnadu, India.

[2]PhD., Professor, Department of Electronics and Communication Engineering, Saveetha School of Engineering, Saveetha Institute of Medical and Technical Sciences, Saveetha University Chennai, India.

* corresponding: kudiyarasan@rediffmail.com

Abstract:

In general, symmetrical and asymmetrical capacitor-clamped boost converters and direct current capacitor voltage, unbalancing specially with lower output current Total Harmonic Distortion are frequent problems for inverters. In order to improve voltage quality, a boost converter with a flying capacitor and grid tie inverter is suggested in this study. It manages the direct current link voltage asymmetrically. Additionally, the boost converter with flying capacitor grid tie inverter system's output voltage dynamic responses are enhanced and simulated using MATLAB Simulink which in turn benchmarked using a scaled-down hardware module. Proportional Integral and Model Predictive Controller control strategies are suggested and implemented in the built hardware. The suggested system's voltage, current, and dynamic performance are examined. The results show that a 360 Watt output power can be delivered by the suggested combination of the described converter system. Additionally, grid-connected power converters and flying capacitor boost converters have lower current harmonics and better voltage regulation direct/alternating current converters, demonstrating the developed system's great suitability for power usage in home photovoltaic systems.

Keywords: Flying Capacitor, Total Harmonics Distortion, Boost Converter, closed loop system, Model predictive controller, grid connected power converters.

1. Introduction

Nowadays, Inverters based on energy sources namely of renewable type are widely used due to their high-power capacity. In multilevel topologies, controlling the number of switching devices and maintaining power quality becomes difficult. To overcome the discussed demerits, several researchers have introduced a new topology namely a multilevel system with a unique topology [1]. Further, the new

Note:- Artificial intelligence tools were used solely for language refinement and formatting support. The technical content, analysis, results, and conclusions were entirely developed by the authors.

modulation technique has been introduced based on the elimination of harmonics in grid-connected power converters with nonlinear load is proposed by using Hysteresis Control (HC) techniques.

The inverter is designed with a power and frequency rating of 120V or 220V and 60Hz or 50Hz, respectively, taking into account the worldwide need for electricity. For Photovoltaic and fuel cell systems, the soft switch Pulse Width Modulation (PWM) in conjunction with the boost converter proves to be an effective combination. The closed loop controls are introduced to improve power quality however, the multilevel switching is nonlinear, and model-free adaptive control is required to meet this demand. To persuade, the sliding mode controls are introduced in the converters, and a series of resonant DC converters are introduced for power factor improvement to de-couple the Electromagnetic Capability (EMC) and Electromagnetic Interference (EMI), the best Light Emitting Diode (LED) drivers are introduced using a novel approach [2].

Several researchers have introduced various boost converters for domestic applications [3-15]. The main challenge in PV systems is maintaining power quality since they produce different harmonics. Passive filters can reduce the amplitude of the harmonics however, in the paper [16], the shunt cascaded systems are used in which another set of inverters injects the harmonic frequencies in the opposite phase to eliminate the influence of harmonics. For appropriate power transfer from the solar cell to the grid, both sides' impedances must be balanced, which is now performed using multilayer inverters and it becomes unstable and introduces THD when a DC bus is swapped. In the paper [17], a comparative examination of several multi-level topologies in closed-loop systems is presented to improve the performance of THD. Furthermore, the current harmonics can be eliminated using a shunt active filter, which injects the harmonic frequency into the system. In the study [18], a flying capacitor for the active power filter and a fuzzy information system are utilized to increase the converter's dynamic response. Also, the voltage level is determined by the carrier shift in the PWM process. In the paper [19], multiple single-phase modules are employed, with a flying capacitor determining the voltage level and cascading it to reach the converter's power and voltage ratings. The design of a DC-DC converter is critical in matching the impedance of the load and source for maximum power transfer. However, the design becomes more challenging when high gain and power are used. In the study [20], an interleaved 3-level boost converter is employed, which is simply a combination of 2 classical boost converters that produce reduced current ripple through the inductor, resulting in superior power quality. Additionally, the flying inductors provide floating electrical parameters that are useful for impedance matching between the utility grid and the converters in the DC-DC operation. However, due to the nonlinear components, system tuning becomes

Note:- Artificial intelligence tools were used solely for language refinement and formatting support. The technical content, analysis, results, and conclusions were entirely developed by the authors.

extremely challenging while operating in closed-loop mode. In the research [21], a model-free adaptive technique is used in which the system can take a non-linearized gain factor to increase the power quality.

At times, the flying capacitor generates some unbalanced floating voltage, which causes harmonic distortion in the power system. In the work [22], the switch capacitors are used in a step-down inverter which eventually increases electricity pumping to the system while minimizing power distortion. Also, the flying capacitor primarily functions as a voltage multiplier in multilevel inverters however, aging can cause power quality issues. In the study [23], a mechanism for balancing the distribution of floating voltage is discussed to enable normal operation with a proportional neutral PWM converter. The flying capacitor is an optimum method for a multi-level inverter to shift the voltage level from a common DC bus since it provides floating ground. To generate an 8-level voltage converter, a special topology is used in which the corresponding flying capacitor is switched [24]. Due to its optimum form factor, reduced components count, better ability to match the impedance between the source and the load to lesser ripple values in the voltage and current, and better dynamic performance in voltage and current regulation, presently, the Flying Capacitor (FC)-based DC-DC converters are required in PV systems in significantly higher quantities [25-26]. Ye et al. (2022) [25] have demonstrated an imbalance in the voltage of flyback capacitor multilevel converters in real-time scenarios. Zhao et al. (2021) [26] have proposed a synchronous phase shifting decoupling method to avoid neutral point voltage and coupling of the system. By incorporating model predictive control into smart grid systems, this effort seeks to validate the idea of improved dynamic responsiveness and improved power quality.

The objective of this work is to propose a boost converter with a flying capacitor and a grid-tied inverter to enhance voltage quality and reduce current harmonics under smart grid operation. Although flying capacitor converters and advanced control techniques have been previously reported, the fundamental novelty of this work lies in the combined implementation of an asymmetrically regulated DC-link flying capacitor boost converter with a cascaded filtering structure and a model predictive control (MPC) strategy, validated through both simulation and hardware experimentation. Unlike the single-stage flying inductor buck–boost inverter reported in [21], the proposed system employs a two-stage FC boost converter with cascaded filtering, enabling superior ripple suppression and dynamic voltage regulation. In contrast to [25], which primarily addresses capacitor voltage imbalance phenomena, this work demonstrates practical harmonic mitigation and transient performance improvement under grid-connected power converter conditions. Furthermore, while balancing-oriented control approaches are discussed in [26], the present study focuses on asymmetrical DC-link voltage regulation aimed at power quality enhancement and fast dynamic response. The key contributions of this work are summarized as follows:

Note:- Artificial intelligence tools were used solely for language refinement and formatting support. The technical content, analysis, results, and conclusions were entirely developed by the authors.

10.22060/EEJ.2026.24986.5808

- Developed a boost converter with a flying capacitor grid tie inverter system and its voltage THD & current THD have been analyzed.
- Two different control strategies namely PI and MP have been implemented in the proposed system.
- The PI and MP closed-loop control algorithms have been deployed in the developed prototype hardware and the best control strategy is identified by analyzing its dynamic performance.

2. Methodology

The block diagram of the existing dc-ac converter is shown in Fig.1. Further, the circuit diagram of the H-Bridge inverter with a flyback capacitor, where the load side is matched by an LC filter is shown in Fig.2. The existing system consists of a DC source, single stage boost converter, an inverter, an LC filter and a load.

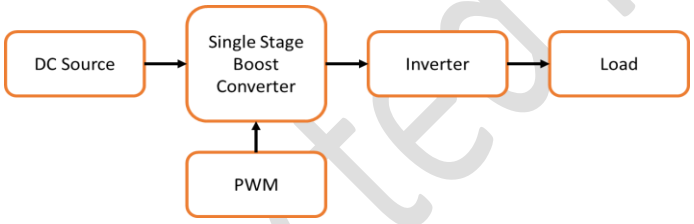

Fig.1. Existing block diagram

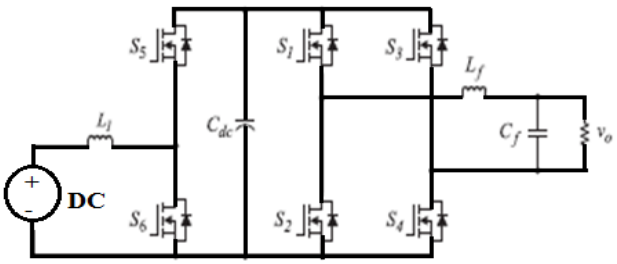

Fig.2. Existing circuit diagram

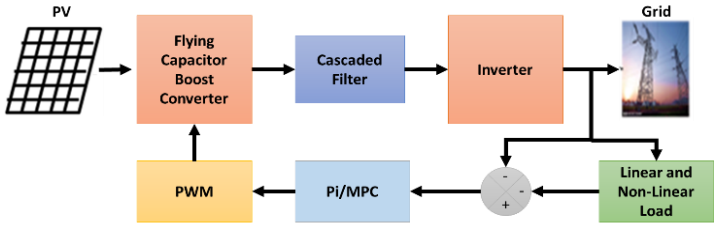

Note:- Artificial intelligence tools were used solely for language refinement and formatting support. The technical content, analysis, results, and conclusions were entirely developed by the authors.

Fig.3.Proposed closed-loop simulation with model predictive controller

The closed loop grid tie system's architecture is explained in Fig. 3. Fig. 4 shows the Gretel inverter with a C filter and the flyback capacitor-based boost converter. There are several factors such as grid voltage fluctuations, grid frequency changes, grid faults & disturbances etc. which affect the inverter voltage when it is connected to the grid. Regardless of controlling the DC link voltage, which in turn maintains the output voltage level, it is crucial to estimate the inverter output and current.

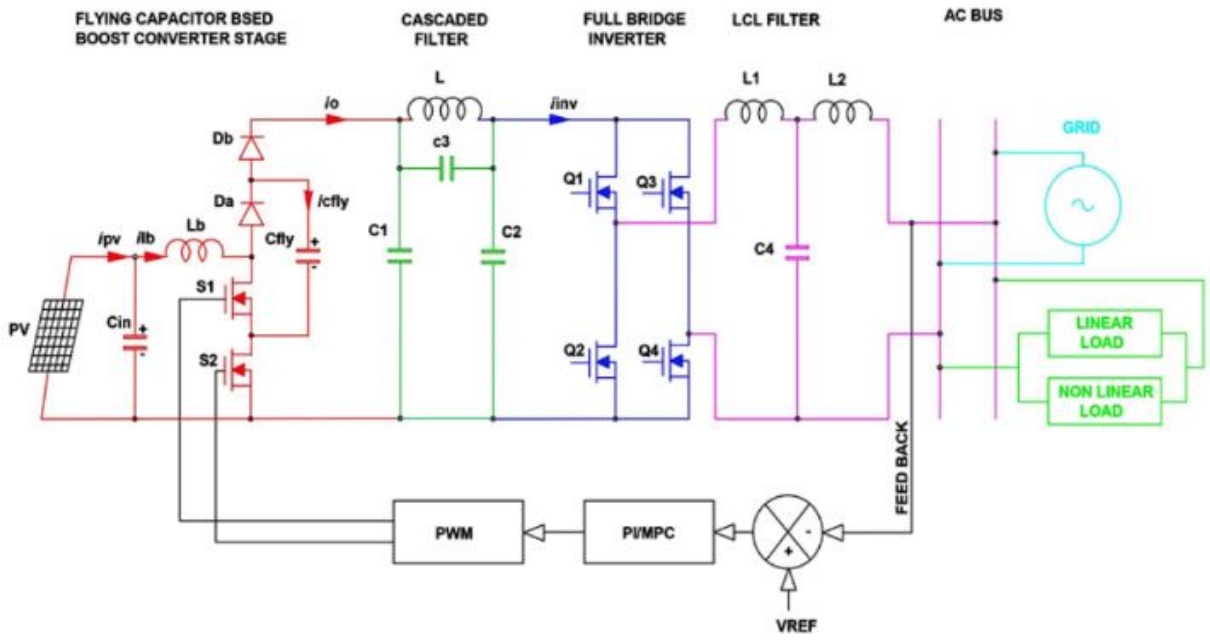

Fig.4. Circuit diagram of closed loop-controlled PV grid-connected system

Even though several classical and advanced control techniques are available for AFE control, the dynamic requirements for power system identification in such cases become more complicated, or the transfer function is involved with higher order terms, resulting in nonlinearity in the system, which is a limitation in classical control in such cases and for PV applications. The load current and the power sink parameter are completely dependent on the converter DC link voltage, which must be maintained stable by considering the dynamic change of the system demand with a Model Predictive Control (MPC), which can adopt nonlinear gain factors to meet the requirement.

Note:- Artificial intelligence tools were used solely for language refinement and formatting support. The technical content, analysis, results, and conclusions were entirely developed by the authors.

10.22060/EEJ.2026.24986.5808

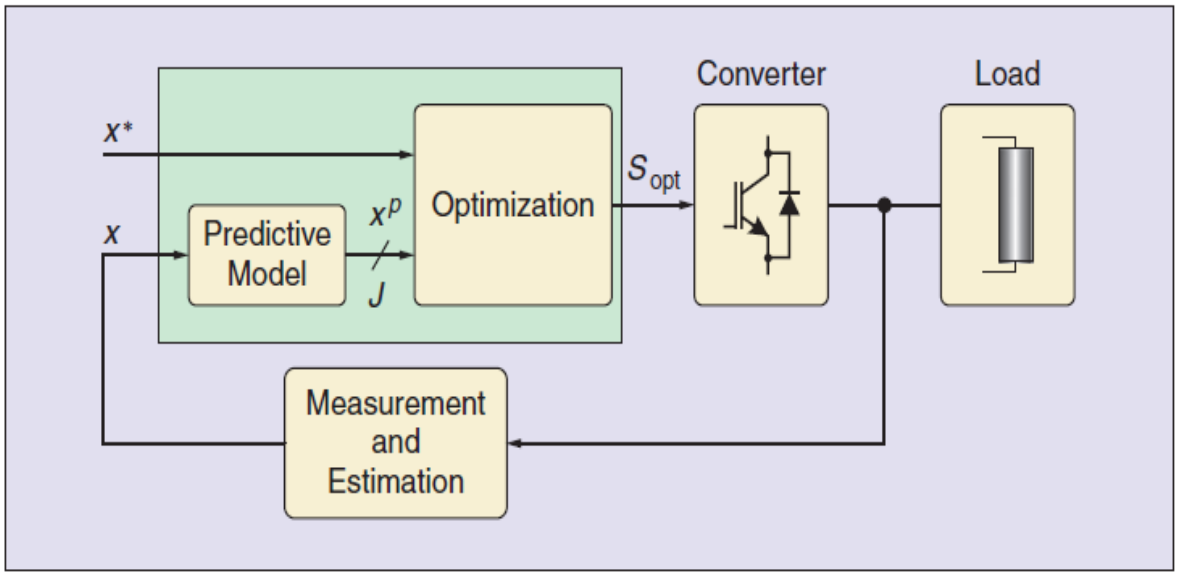

Fig.5. Block diagram of advanced control with nonlinear gain factors

In contrast to conventional control, the suggested controller can take error and its derivative, which can then be used to oppose system excitation for improved dynamic responsiveness and to meet the requirements of a dynamic power compensator.

Although the proposed flying capacitor (FC) boost converter shares certain structural similarities with existing FC-based multilevel converters, its distinguishing features lie in the combined use of a two-stage boost configuration, asymmetrical DC-link voltage regulation, cascaded filtering, and a model predictive control (MPC) strategy aimed at improving dynamic response and power quality.

To clearly highlight the structural and performance advantages of the proposed topology over existing FC-based converters, a comparative analysis with recent state-of-the-art designs is presented in Table 1. The comparison considers key aspects such as component count, voltage stress, control complexity, efficiency, and harmonic performance.

Note:- Artificial intelligence tools were used solely for language refinement and formatting support. The technical content, analysis, results, and conclusions were entirely developed by the authors.

10.22060/EEJ.2026.24986.5808

Table 1: Comparison of Flying Capacitor-Based Converter Topologies and Proposed Two-Stage Boost Design

Reference	Converter Type	Active Switches	Flying Capacitors	Voltage Stress	Control Strategy	Efficiency (%)	Voltage THD (%)	Key Focus
[21]	Single-stage flying inductor buck–boost inverter	Moderate	None	High	PI-based control	92.1	3.8	Voltage gain improvement
[25]	FC multilevel DC–DC converter	High	Multiple	Moderate	Balancing control	93.4	3.2	Capacitor voltage balancing
[26]	FC-based boost converter	Moderate	Single	Moderate	Conventional PI	94	2.9	DC-link voltage balance
Proposed	**Two-stage FC boost converter with cascaded filter**	**Moderate**	**Single**	**Reduced**	**Model Predictive Control**	**95.6**	**1.92**	**Dynamic response & power quality**

As observed from Table 1, the proposed topology achieves lower voltage stress across the power switches while using fewer flying capacitors compared to multilevel FC converters reported in [25] and [26]. Unlike [21], which employs a single-stage topology with limited harmonic suppression capability, the proposed 2-stage configuration with cascaded filtering significantly improves voltage and current quality. Furthermore, the use of MPC enhances dynamic response and reduces harmonic distortion without

Note:- Artificial intelligence tools were used solely for language refinement and formatting support. The technical content, analysis, results, and conclusions were entirely developed by the authors.

10.22060/EEJ.2026.24986.5808

increasing circuit complexity, thereby offering a balanced trade-off between performance and implementation cost.

3. Mathematical modelling of boost converter and flying capacitor boost converter

Fig. 6 depicts a single photovoltaic cell equivalent circuit, but a PV module will be made up of numerous PV cells which are connected in two different configurations namely series and parallel depending on the power need. The photon source current I_{ph} is determined by the irradiation, as shown in equation (1), and the reverse saturation current is related to the short circuit current, as shown in equation (2). Equation (3) represents the total cell saturation current. The instantaneous total module current is described by equation (4).

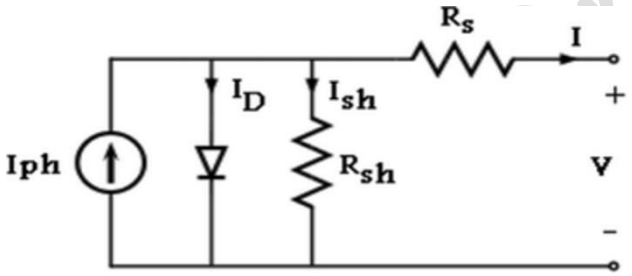

Fig.6. Photovoltaic cell equivalent circuit

$$I_{ph} = [I_{sc} + K_i(T - 298)] \frac{I_r}{100} \quad (1)$$

$$I_{rs} = \frac{I_{se}}{[e^{(\frac{qV_{oc}}{N_s K_n T})} - 1]} \quad (2)$$

$$I_o = I_{rs} \left(\frac{T}{T_r}\right)^3 e^{[\frac{qE_{go}}{nK}(\frac{1}{T} - \frac{1}{I_r})}} \quad (3)$$

$$I = N_p I_{ph} - N_p I_o \left(e^{\frac{\left(\frac{V}{N_s} + \frac{IR_s}{N_p}\right)}{nV_t}} - 1 \right) - I_{sh} \quad (4)$$

Note:- Artificial intelligence tools were used solely for language refinement and formatting support. The technical content, analysis, results, and conclusions were entirely developed by the authors.

10.22060/EEJ.2026.24986.5808

where $V_t = \frac{KT}{q}$ and $I_{sh} = \frac{\left(\frac{VN_p}{N_s} + I_{rs}\right)}{R_{sh}}$

K_i = Short circuit current at 25°C, 1000 w/m^2

N_s = No. of cell in series

n = Diode ideality factor

I_{rs} = Reverse saturation current

K = Boltsman contant

T = Insantanious temperature

T_r = Reference temperature

E_{go} = Band Gap

I_{ph} = Photon current

I_{sh} = Shunt current

I_o = Reverse saturation current of cell

N_p = No. of parallel paths

R_s = Series resistance

I = Total instatanious PV module current

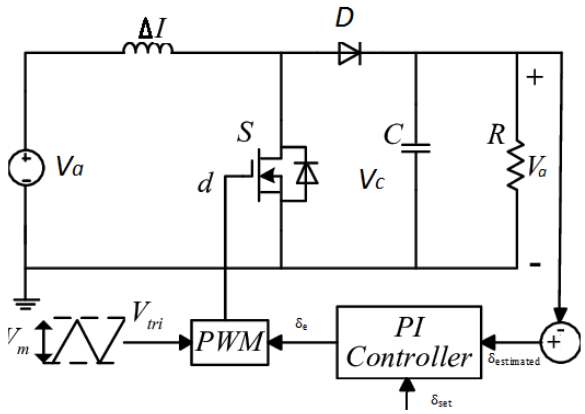

Note:- Artificial intelligence tools were used solely for language refinement and formatting support. The technical content, analysis, results, and conclusions were entirely developed by the authors.

10.22060/EEJ.2026.24986.5808

Fig.7 Boost converter in closed-loop operation

The closed-loop control of a boost converter is shown in Fig. 7. The output voltage is simply the voltage across the capacitor, as defined in equation (8), and the output voltage relationship is determined by the duty cycle, as defined in equation (5). The ripple current through the inductor is computed to determine the critical size of the inductor, which is provided by equation (6). The current ripple is determined by the OFF time, which is provided in equation (7). The performance of the converter is reliant on the estimation of crucial inductor and capacitor sizes, as given in Equation (9) and Equation (10).

$$V_a = \frac{V_s}{1-K} \tag{5}$$

$$\Delta I = \frac{(V_a - V_s)t_2}{L} \tag{6}$$

$$T = t_1 + t_2 = \frac{\Delta I L}{V_s} + \frac{\Delta I L V_a}{V_a - V_s} \tag{7}$$

Where $t_1 = KT$, $t_2 = (1-K)T$,

$$\Delta V_c = \frac{1}{c}\int_0^{t_1} I_c \, dt \tag{8}$$

$$L = \frac{K(1-K)R}{2f} \tag{9}$$

$$\frac{KV_s}{fL} = \frac{2V_s}{(1-k)R} \tag{10}$$

V_a = Output voltage

V_s = Input Voltage

V_c = Capacitance ripple

K = Duty cycle

L = Series inductance

ΔI = Inductance current ripple

$t_1 = ON\ Time$

$t_2 = OFF\ Time$

Note:- Artificial intelligence tools were used solely for language refinement and formatting support. The technical content, analysis, results, and conclusions were entirely developed by the authors.

10.22060/EEJ.2026.24986.5808

A closed loop of a boost converter requires feedback to estimate the converter's duty cycle, for which output voltage feedback is used. The duty cycle is estimated in equation (12), and the error is estimated in equation (11), which serves as the excitation for the PI regulator. Equations (13) and (14) describe the output duty cycle based on PI tuning. The converter's instantaneous output is stated in equation (15).

$$\delta_e = \delta_{set} - \delta_{estimated} \quad (11)$$

$$\delta_{estimated} = \frac{t_1}{T} \quad (12)$$

$$K = K_p \delta_e + K_i \int \delta_e \, dt \quad (13)$$

$$V_a = \frac{V_s}{1-K} \quad (14)$$

$$\frac{KV_s}{fL} = \frac{2V_s}{(1-K)R} \quad (15)$$

$\delta_e =$ Excitation error

$\delta_{set} =$ Duty ratio set value

$\delta_{estimated} =$ Estimated feed back

$K_p = Proportional\ constant$

$K_i = Integral\ Constant$

The voltage conversion ratio (VCR) of the Flying Capacitor Boost DC-DC Converter is given in Equation (16).

$$\frac{V_a}{V_s} = \frac{1}{1-K} \quad (16)$$

The energy storage element namely inductor of the flying capacitor boost converter (FCBC) shall be given in equation (17).

$$L_{FCBC} = 0.25\ L_{boost} \quad (17)$$

Also, the volume of the FCBC is given in equation (18)

$$Vol_{(3-levels)} = 0.35\ Vol_{existing} \quad (18)$$

Note:- Artificial intelligence tools were used solely for language refinement and formatting support. The technical content, analysis, results, and conclusions were entirely developed by the authors.

10.22060/EEJ.2026.24986.5808

The value of inductor, inductor current ripple and capacitor of FCBC can be given in equation(19)(20) and (21).

$$L = \frac{V_s K}{4 \Delta I_s f_{sw}} \quad (19)$$

$$\Delta i_L = \frac{V_s (V_a - 2V_s)}{2 L f_{sw} V_a} \quad (20)$$

$$C = \frac{V_a}{2 R \Delta V_c f_{sw}} \quad (21)$$

3.1. Asymmetrical DC-Link Voltage Control Strategy

In conventional DC-link regulation schemes, the voltages across multiple DC-link capacitors are maintained symmetrically, such that each capacitor shares an equal portion of the total DC-link voltage. In contrast, asymmetrical DC-link voltage control is defined in this work as the intentional and controlled regulation of unequal voltage distribution across the DC-link capacitors in order to enhance transient energy redistribution, improve dynamic response, and reduce harmonic distortion under grid-connected power converted operation.

3.1.1. Mathematical Justification

Considering a two-capacitor DC-link structure with flying capacitor assistance, the total DC-link voltage Vdc is expressed in equation (22):

$$Vdc = VC1 + VC2 \quad (22)$$

where VC1 and VC2 denote the voltages across the upper and lower DC-link capacitors, respectively.

In conventional symmetric control, objective is assumed as VC1=VC2=Vdc2.

However, in the proposed asymmetrical DC-link voltage control, the regulation objective is intentionally modified as VC1≠VC2 (equation (23)),subject to

$$VC1 + VC2 = Vdc \quad (23)$$

This asymmetric voltage distribution enables flexible energy buffering and faster redistribution of stored energy during transient operating conditions such as load changes and grid disturbances.

3.1.2. Control Objective and Duty-Cycle Interaction

The duty cycle ddd of the boost stage directly influences the charging and discharging behavior of the DC-link capacitors. Under asymmetrical control, the duty-cycle command is dynamically

adjusted to regulate VC1 and VC2 independently, thereby modifying the effective voltage gain and transient response characteristics of the converter.

By allowing controlled deviation from symmetrical voltage sharing, the proposed method improves the converter's ability to respond rapidly to reference changes while simultaneously reducing voltage ripple propagation to the grid-side inverter.

3.1.3. Distinction from Conventional DC-Link Regulation

Unlike conventional symmetric DC-link regulation methods, which prioritize voltage balancing alone, the proposed asymmetrical DC-link voltage control introduces an additional degree of freedom in the control strategy. This flexibility enables improved dynamic performance and enhanced harmonic suppression without increasing circuit complexity or component count. The effectiveness of this approach is further enhanced when combined with the predictive nature of the MPC strategy, which anticipates future voltage states and compensates for nonlinear system dynamics.

4. Simulation Results

In this work, two different simulation works namely Open loop simulation and Closed loop simulation and one experimental evaluation is done to analyze the performance of the proposed system.

4.1 Open loop simulation results

Fig. 8 (a) depicts the design of a C filter-based DC converter and a half-controlled grid tie inverter, while Fig. 8 (b).

Note:- Artificial intelligence tools were used solely for language refinement and formatting support. The technical content, analysis, results, and conclusions were entirely developed by the authors.

10.22060/EEJ.2026.24986.5808

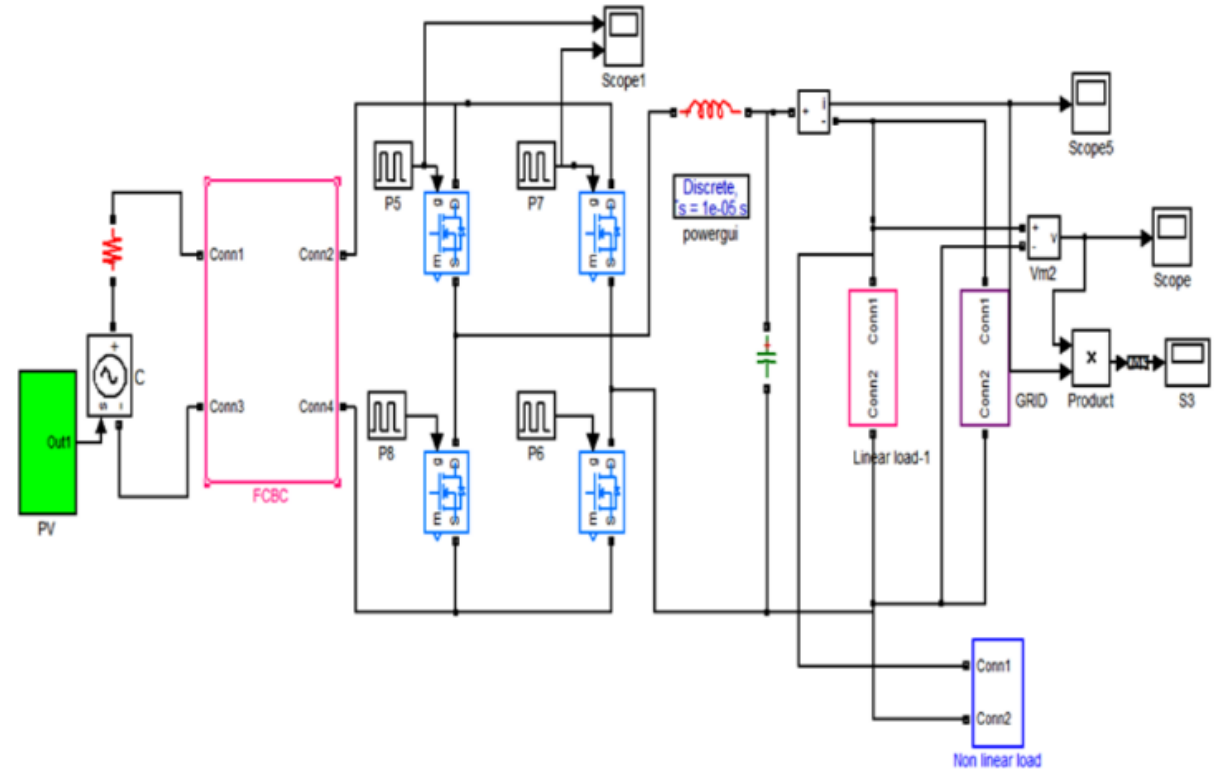

(a)

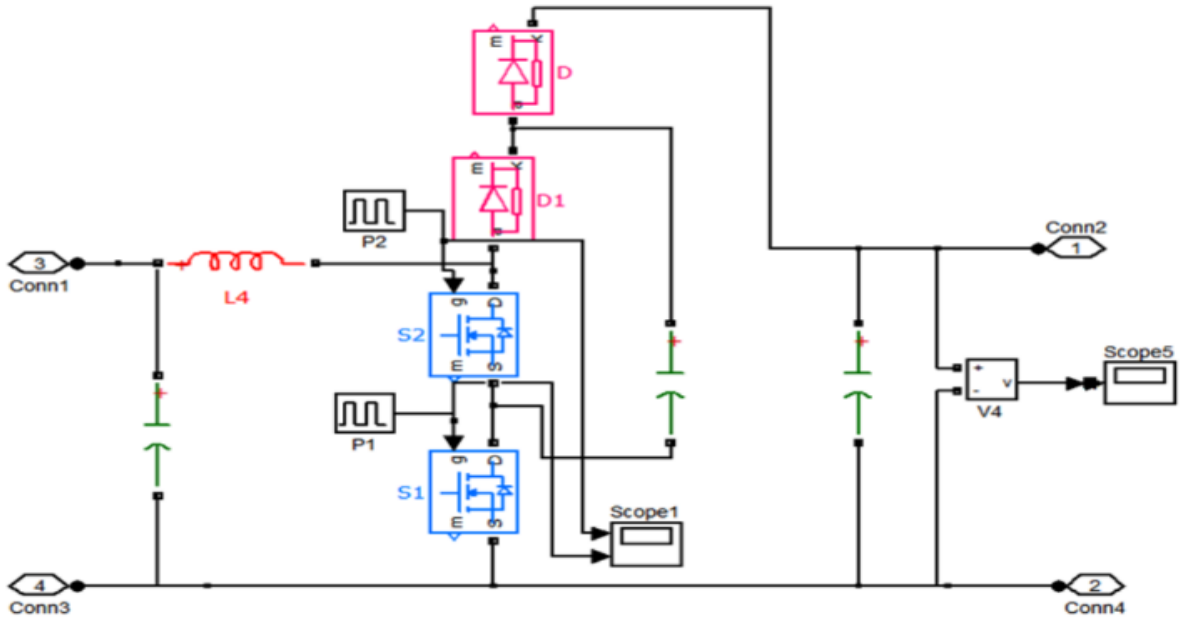

(b)

Fig.8. (a) Boost converter with flying capacitor circuit diagram and grid tie connection with C filter (b) Grid Connection

Note:- Artificial intelligence tools were used solely for language refinement and formatting support. The technical content, analysis, results, and conclusions were entirely developed by the authors.

10.22060/EEJ.2026.24986.5808

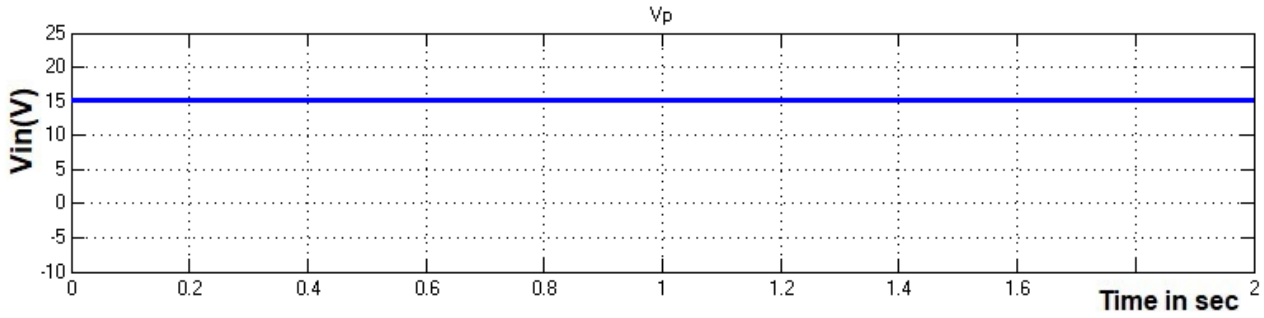

Fig.9. Input voltage of flying capacitor-based DC-DC Converter with C filter

The voltage across PV is shown graphically in Fig. 9 and its value is 15 Volts. Further, the switching pulse of the FC-boost converter appears in shown in Fig.10 and it is seen that the normalized value is shown as 1.

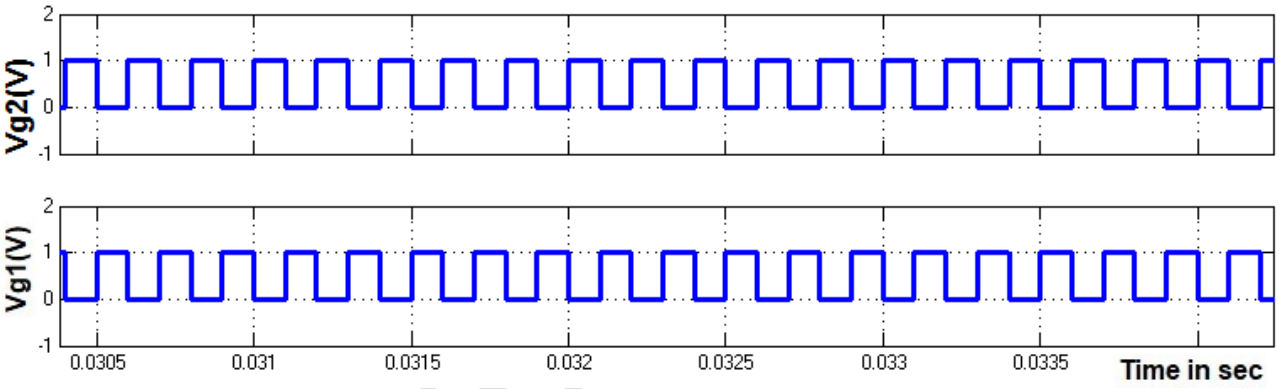

Fig.10. MOSFET Gate Pulses of FC-boost converter with C-filter

The output voltage across the FC-boost converter is shown in Fig. 11 and its value is 60 Volts. Further, it is observed that the Ripple Voltage across of FCC-boost converter is 1.2 V and as shown in Fig.12. Also, the current through RL load is shown in Fig.13.

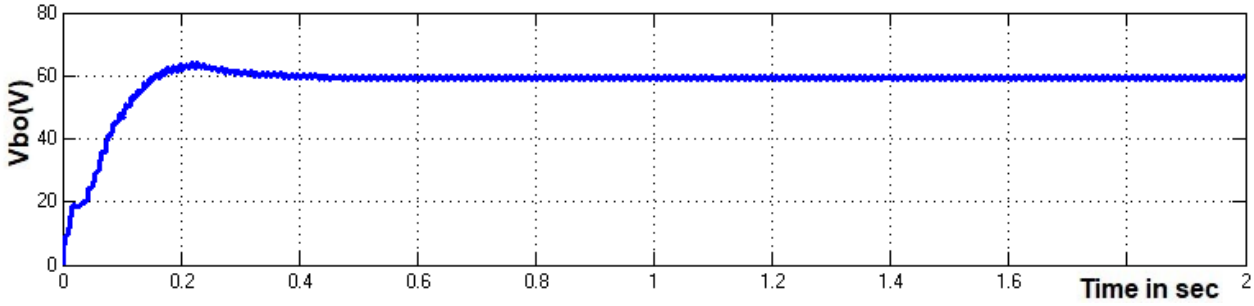

Fig.11. Voltage across FC boost converter with C-filter

Note:- Artificial intelligence tools were used solely for language refinement and formatting support. The technical content, analysis, results, and conclusions were entirely developed by the authors.

10.22060/EEJ.2026.24986.5808

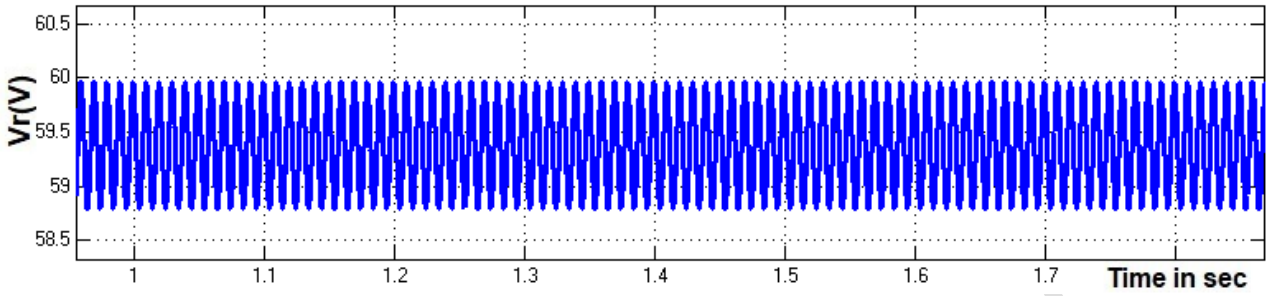

Fig.12. Ripple voltage across FC boost converter with C-filter and grid-connected inverter system

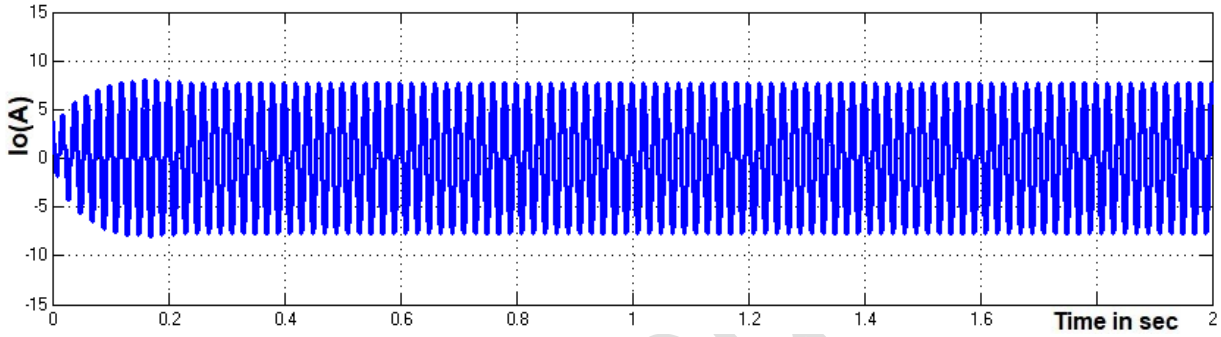

Fig.13. Current through RL load of FC boost converter with C-filter and grid tie inverter system

The current THD of the FC-boost converter is shown in Fig.14. It is seen that the current THD of the FCC-boost converter is 6.45%. Also, the output power of the FCC-boost converter is shown in Fig.15.

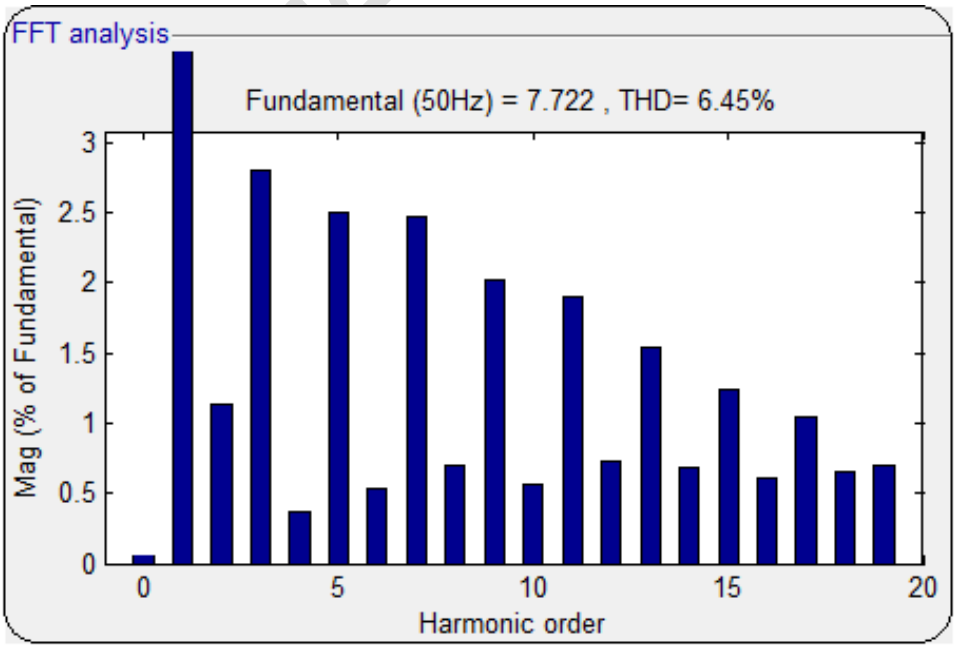

Note:- Artificial intelligence tools were used solely for language refinement and formatting support. The technical content, analysis, results, and conclusions were entirely developed by the authors.

10.22060/EEJ.2026.24986.5808

Fig.14. Current THD of FC-boost converter with C-filter

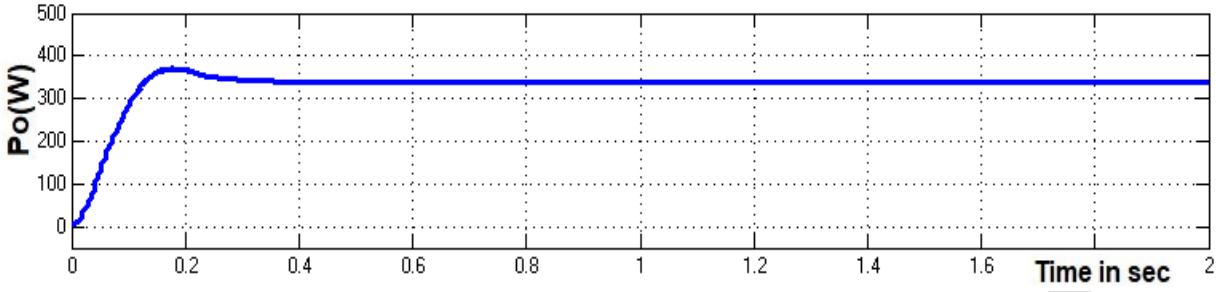

Fig.15. Output power of FC-boost converter with C-filter and grid-connected inverter system

The circuit diagram of the FC-boost converter and grid-connected inverter system with a cascaded filter is shown in Fig. 16. Further, the voltage across the PV input source is shown in Fig.17 and it is seen that the input voltage is 15 Volts.

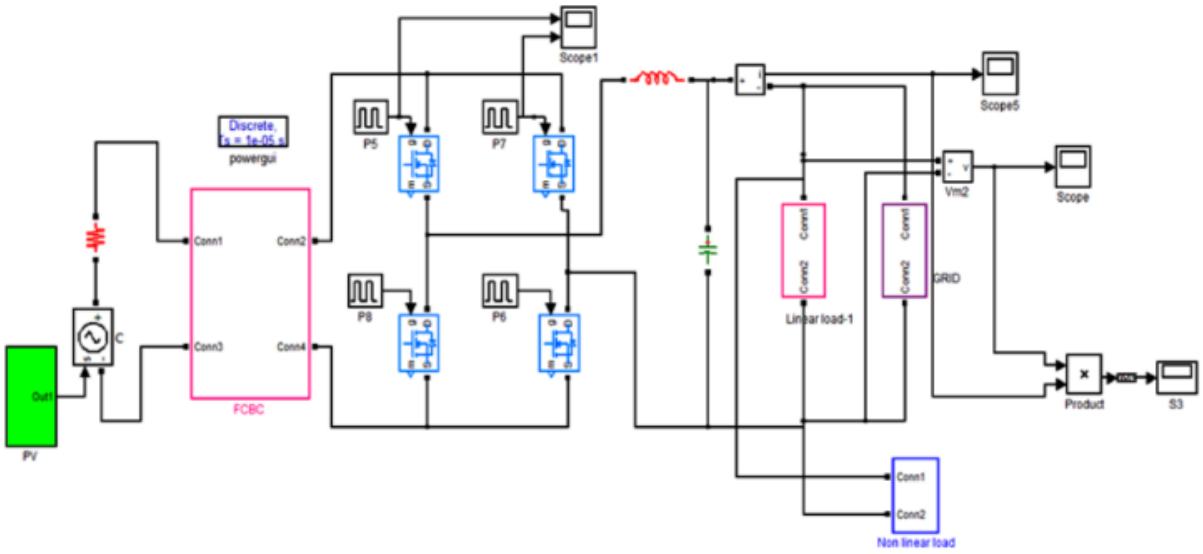

Fig.16. Flying capacitor-based DC-DC Converter and H bridge inverter grid tie inverter with series L and cascaded C filter

Note:- Artificial intelligence tools were used solely for language refinement and formatting support. The technical content, analysis, results, and conclusions were entirely developed by the authors.

10.22060/EEJ.2026.24986.5808

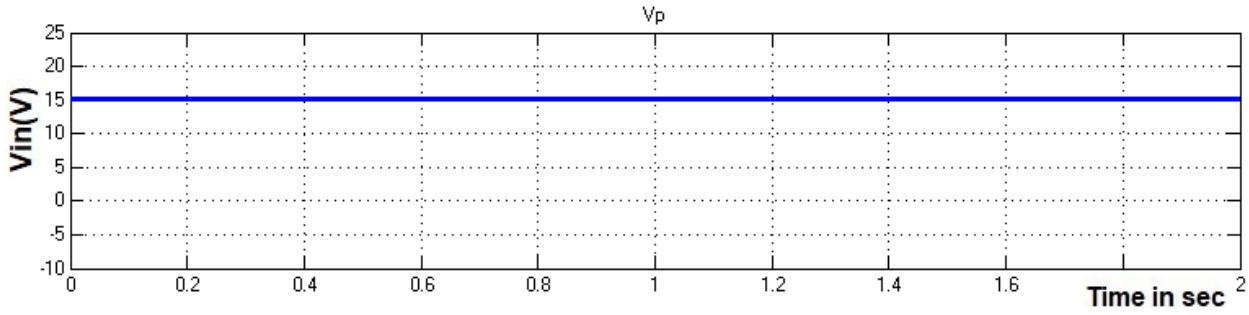

Fig.17. Input voltage of the boost converter with flying capacitor and cascaded filter.

The switching pulse of the FC-boost converter is shown in Fig.17 and it is observed that the normalized value is 1. Also, the switching pulse for the switches S1 and S2 of the flying capacitor boost converter is shown in Fig.18.

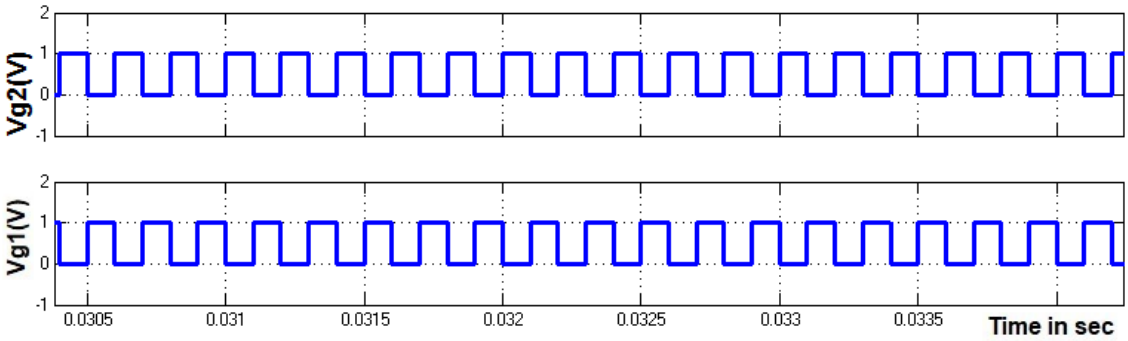

Fig.18. Complementary pulses for flying capacitor-based DC-DC Converter for the switch S1 and S2

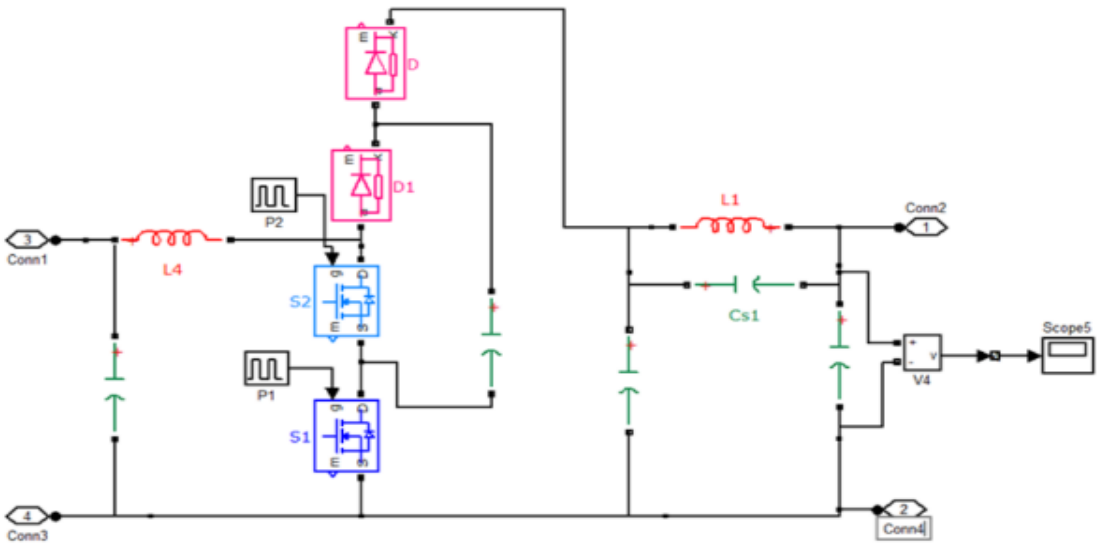

Fig.19. Half-controlled flying capacitor-based DC-DC converter with series L and cascaded C filters.

Note:- Artificial intelligence tools were used solely for language refinement and formatting support. The technical content, analysis, results, and conclusions were entirely developed by the authors.

10.22060/EEJ.2026.24986.5808

Fig.19 shows the circuit diagram of the flying capacitor boost converter with cascaded filter. Further, the voltage across of FCC-boost converter is shown in Fig.20 and its value is 62V. Also, the Ripple Voltage across of FC-boost converter is plotted in Fig.21 and its value is 0.5 V.

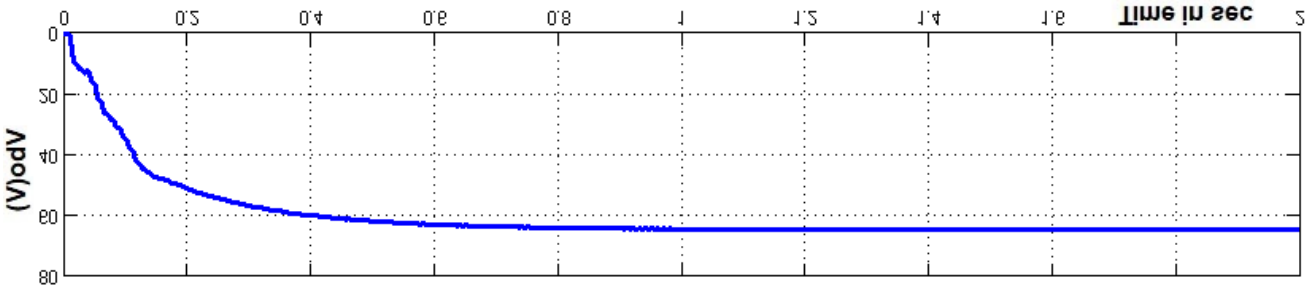

Fig.20. Voltage across FC-boost converter with cascaded filter

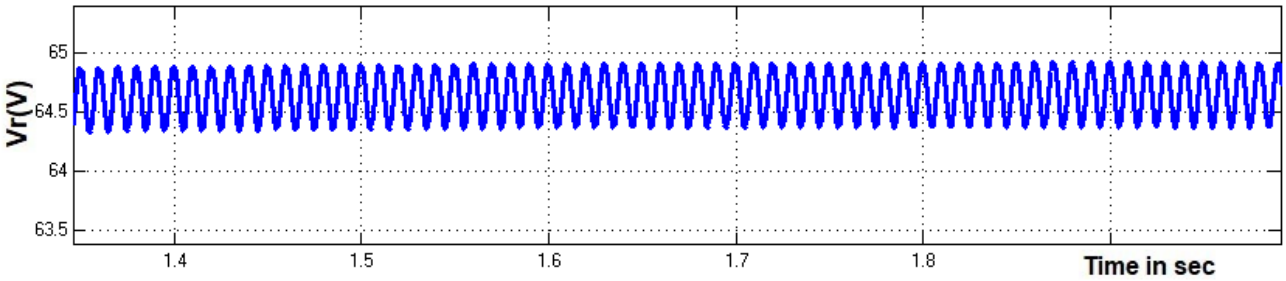

Fig.21. Ripple Voltage across FC-boost converter with cascaded filter and grid-connected inverter system

The switching pulse of the full bridge grid-connected inverter is shown in Figure 22 and its normalized value is observed as 1. Further, the voltage across RL load is shown in Figure 23 and its value is 145V. Also, the current through RL load in Figure 24 and its value is 7.5A.

Note:- Artificial intelligence tools were used solely for language refinement and formatting support. The technical content, analysis, results, and conclusions were entirely developed by the authors.

10.22060/EEJ.2026.24986.5808

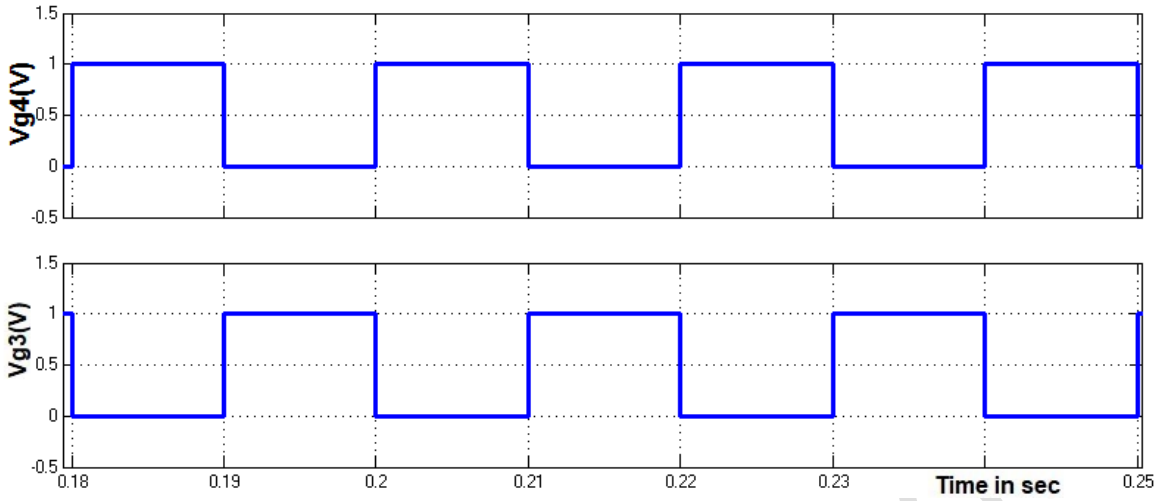

Fig.22. Complementary pulses for the h bridge inverter of switch M3 and M4

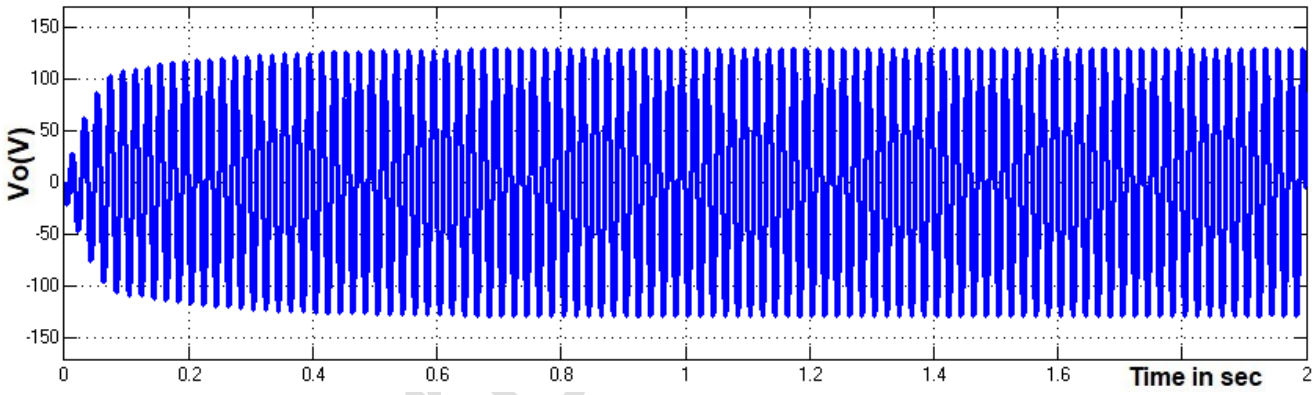

Fig.23. RL load voltage

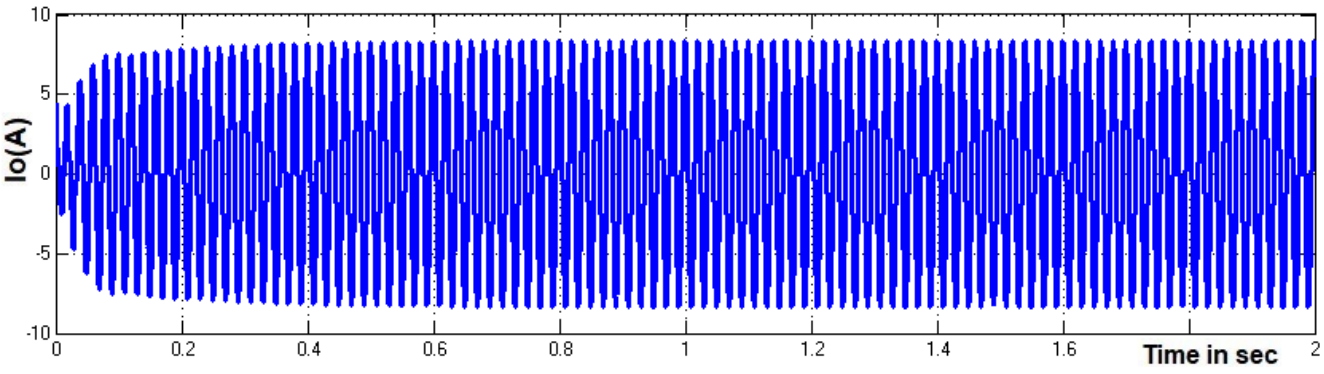

Fig.24. RL load current

Note:- Artificial intelligence tools were used solely for language refinement and formatting support. The technical content, analysis, results, and conclusions were entirely developed by the authors.

10.22060/EEJ.2026.24986.5808

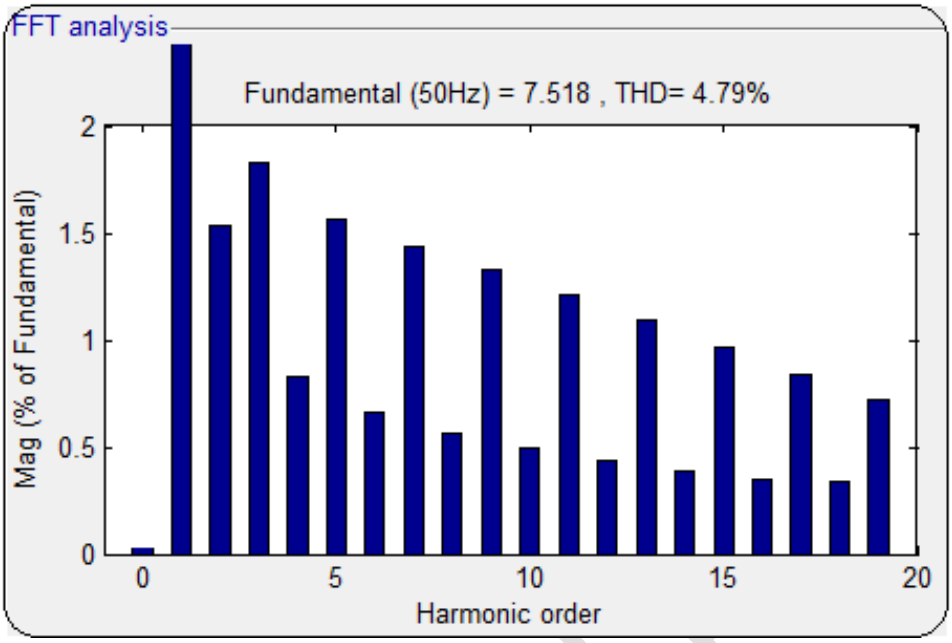

Fig.25. Current THD of FC-boost converter with cascaded filter and grid-connected inverter system

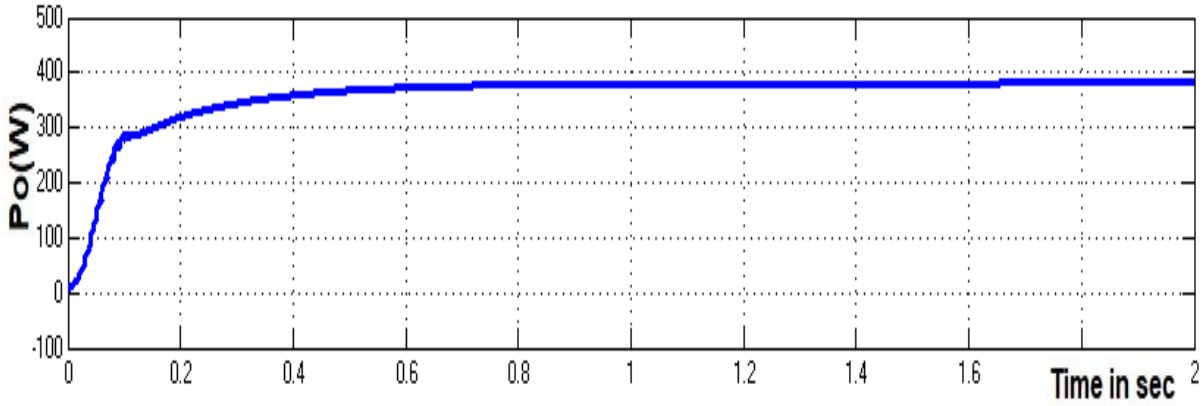

Fig.26. Grid tie inverter with FC-based boost converter power output

The Current THD of the FC-boost converter with cascaded filter and grid-connected inverter system is given in Fig.25 and it is demonstrated that the Current THD value is 4.79%. The power which can be derived from the proposed converter is shown in Fig.26 and its value is 380W. Also, the ripple voltage and output current THD of a flying capacitor boost converter with C-filter and flying capacitor boost converter with Cascaded-filter are compared and the values are presented in Table 2.

Table 2. Comparison of ripple voltage and output current THD

Note:- Artificial intelligence tools were used solely for language refinement and formatting support. The technical content, analysis, results, and conclusions were entirely developed by the authors.

10.22060/EEJ.2026.24986.5808

Flying Capacitor boost and grid connected inverter	Ripple Voltage (V)	Output current THD (%)
C-Filter	1.2	6.45
Cascaded Filter	0.5	4.79

The ripple voltage and output current THD values are from Table 2 and it is demonstrated that the flying capacitor boost converter with a cascaded filter has less ripple voltage and output current THD when compared to the flying capacitor boost converter with C-filter. It is observed that the performance of the flying capacitor boost converter with a cascaded filter is good when compared to the flying capacitor boost converter with a C-filter. So, the flying capacitor boost converter with a cascaded filter is connected to closed-loop PI controller for further analysis.

The results clearly indicate that the flying capacitor primarily contributes to enhanced voltage boosting capability, reduced voltage ripple at the DC-link, and improved transient response during load and reference changes. However, the reduction in output voltage and current total harmonic distortion (THD) is significantly more pronounced when the cascaded LC filter is employed.

While the single C-filter configuration provides limited attenuation of high-frequency switching harmonics, the cascaded LC filter offers superior harmonic suppression by effectively attenuating both low- and high-order components. As a result, the FC boost converter with cascaded LC filtering achieves substantially lower THD values, confirming that the majority of harmonic reduction is attributable to the filter structure rather than the flying capacitor alone.

The comparative THD performance of both configurations is summarized in Table 2, which demonstrates that the cascaded LC filter plays a critical role in meeting grid power quality requirements. Nevertheless, the flying capacitor remains essential for achieving stable voltage regulation and fast dynamic response, thereby complementing the filtering stage rather than replacing it.

4.2 Closed loop simulation results

Fig.27 depicts the proposed control loop in which the inverter output is used as feedback and compared to the desired resonance voltage, resulting in an error that triggers the PI controller and excitation that produces complementary switching pulses for both the inverter and the DC-DC converter. Fig.28 and Fig.29 show the flying capacitor input voltage and its dynamic response, whereas Fig.30 and Fig.31 show the RL load voltage and current, which indicate the effect of switching. Fig.32 depicts the RL load RMS

Note:- Artificial intelligence tools were used solely for language refinement and formatting support. The technical content, analysis, results, and conclusions were entirely developed by the authors.

10.22060/EEJ.2026.24986.5808

voltage, while Fig.33 and Fig.34 indicate the performance of the harmonic voltage and current, with a value of 2.41% and 2.3%, respectively. The efficiency of the proposed system is 94.7% which is derived with the output power of 360 watts whereas the input power is 380 watts. From the analysis, it is observed that the loss of the proposed system is 5.3%. Also, the voltage and current over the RL load are 140V and 8.13A, respectively.

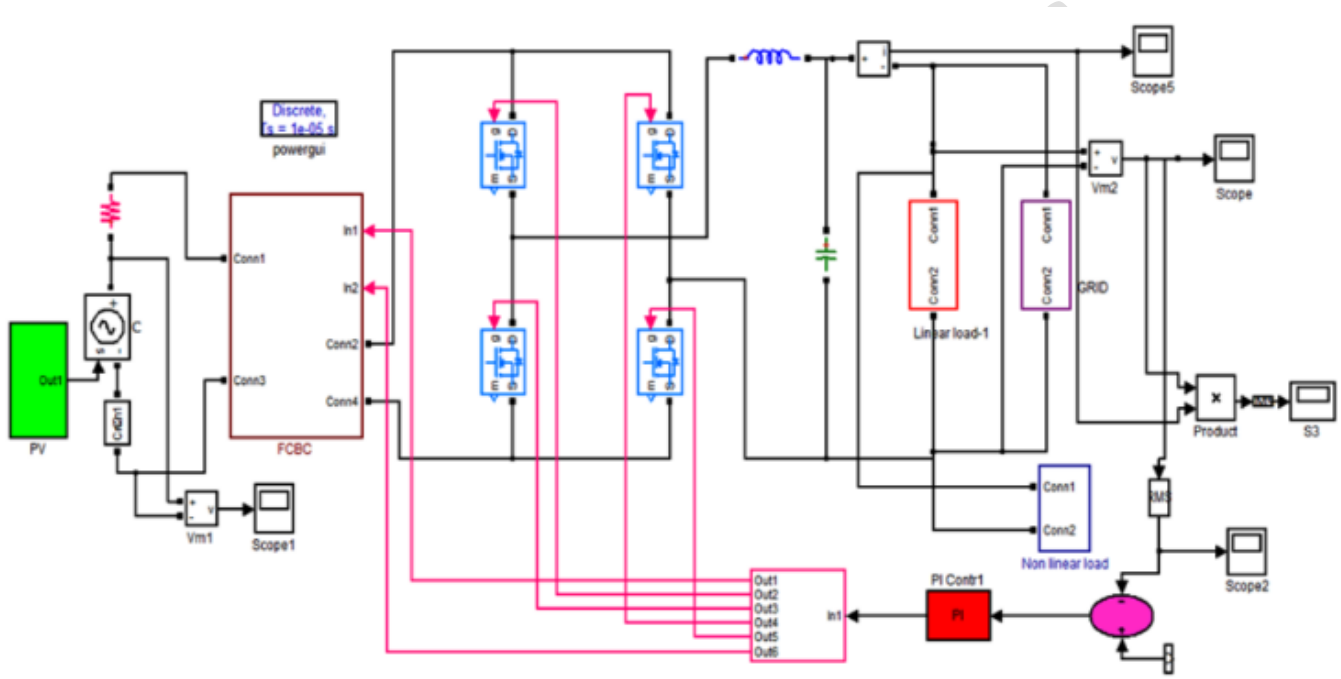

Fig.27. Closed loop PI Control for grid tie inverter and flying capacitor-based DC-DC Converter

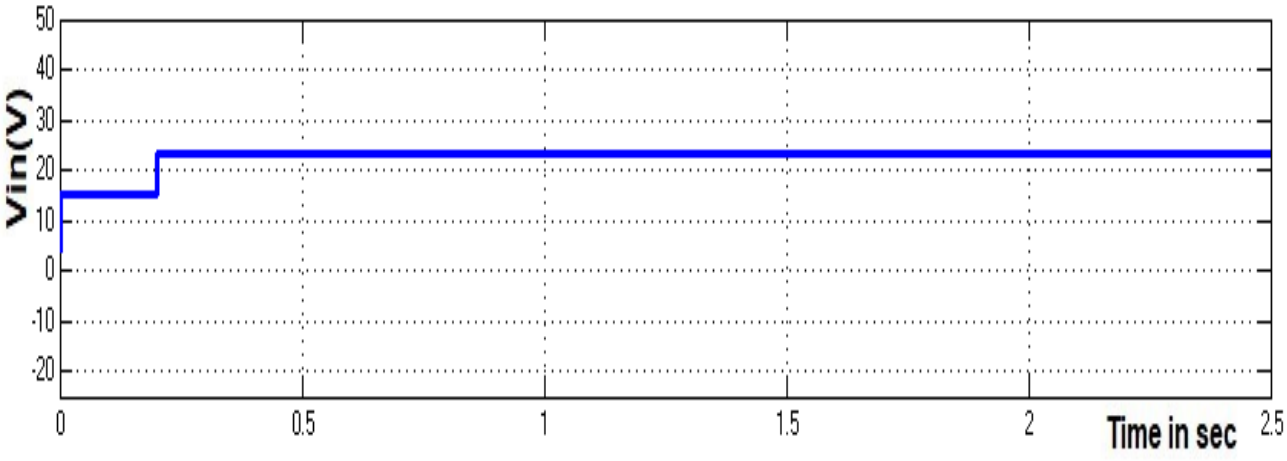

Fig.28. Input voltage of FC-boost converter with a cascaded filter with closed loop PI controller

Note:- Artificial intelligence tools were used solely for language refinement and formatting support. The technical content, analysis, results, and conclusions were entirely developed by the authors.

10.22060/EEJ.2026.24986.5808

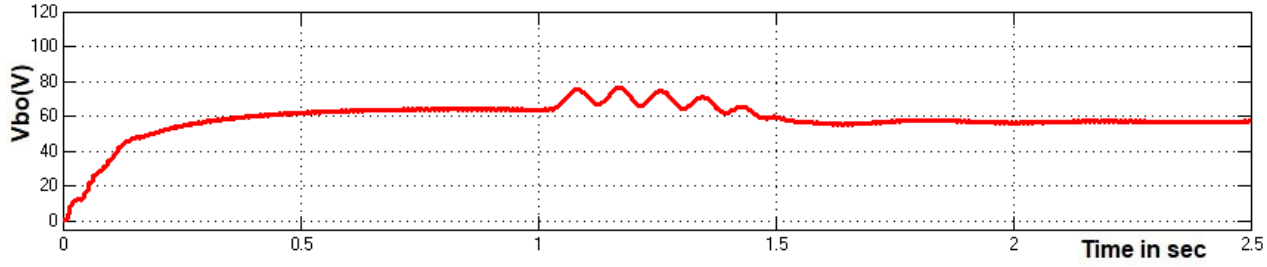

Fig.29. Flying capacitor voltage in DC-DC Converter

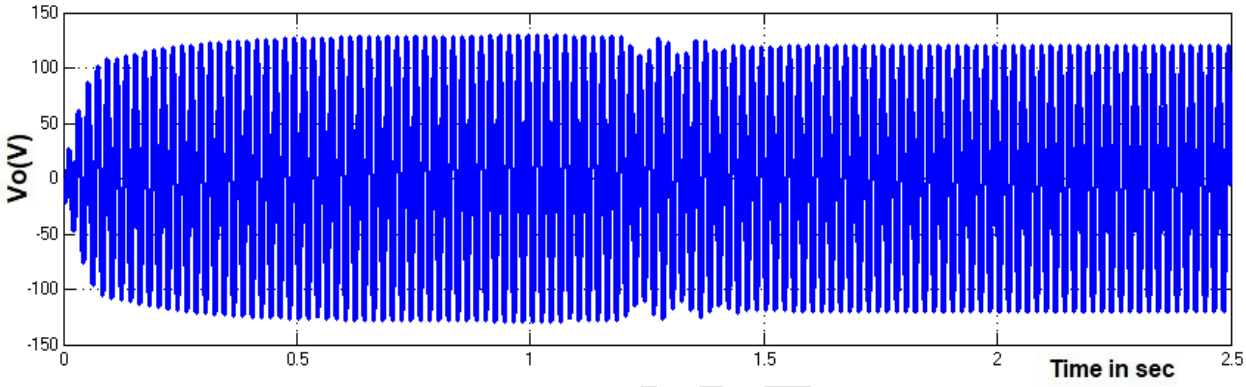

Fig.30. RL load voltage

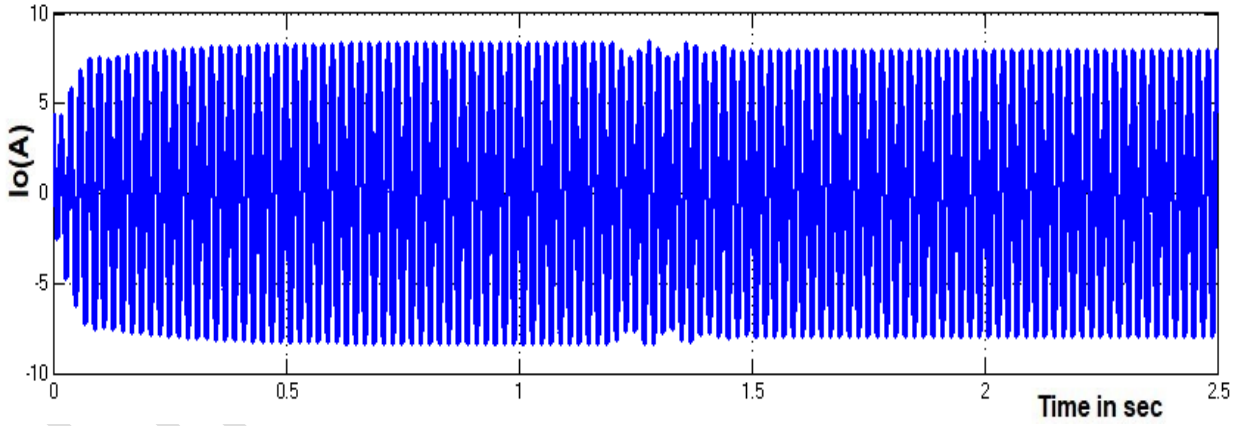

Fig.31. RL load current

Note:- Artificial intelligence tools were used solely for language refinement and formatting support. The technical content, analysis, results, and conclusions were entirely developed by the authors.

10.22060/EEJ.2026.24986.5808

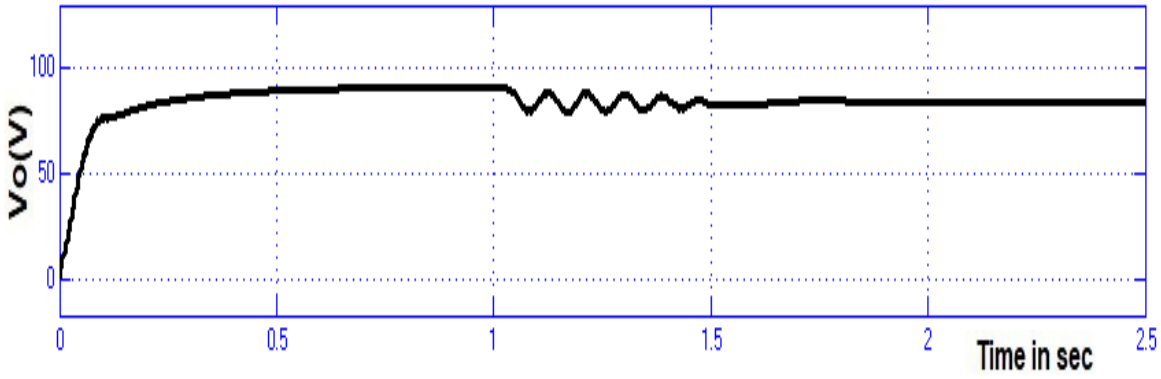

Fig.32. RL load RMS voltage

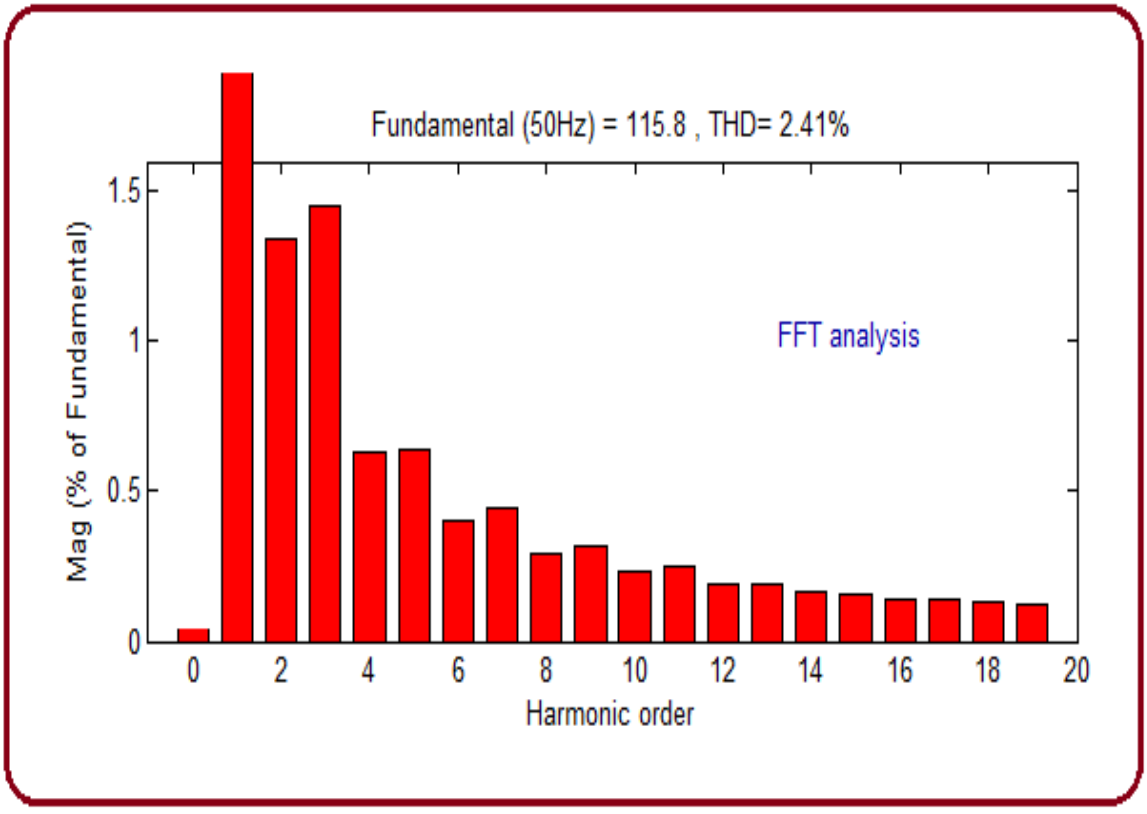

Fig.33. Voltage harmonics

Note:- Artificial intelligence tools were used solely for language refinement and formatting support. The technical content, analysis, results, and conclusions were entirely developed by the authors.

10.22060/EEJ.2026.24986.5808

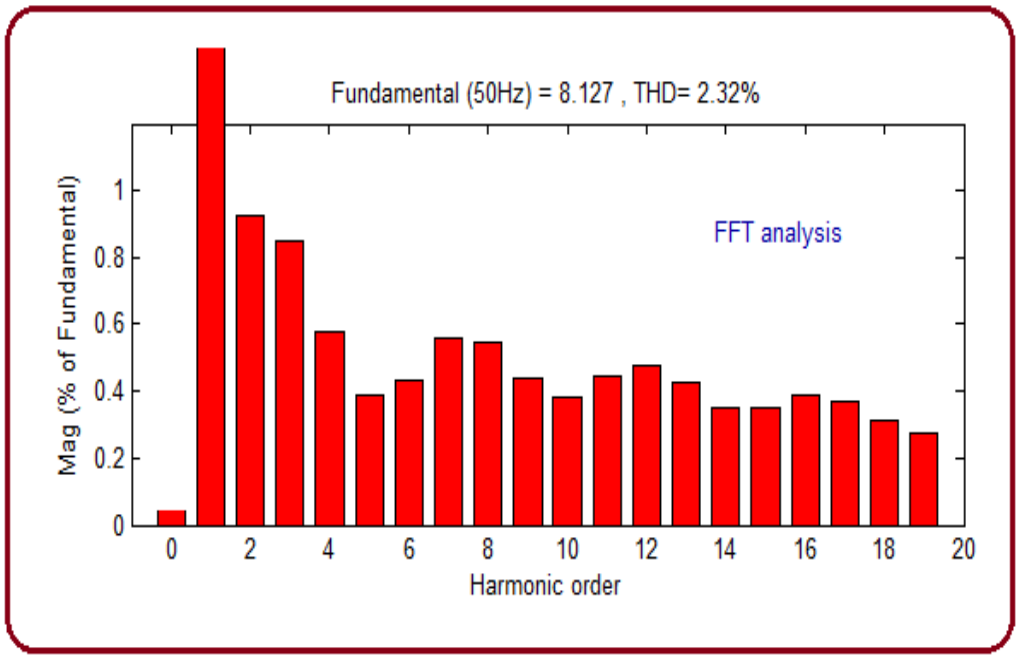

Fig.34. Current harmonics

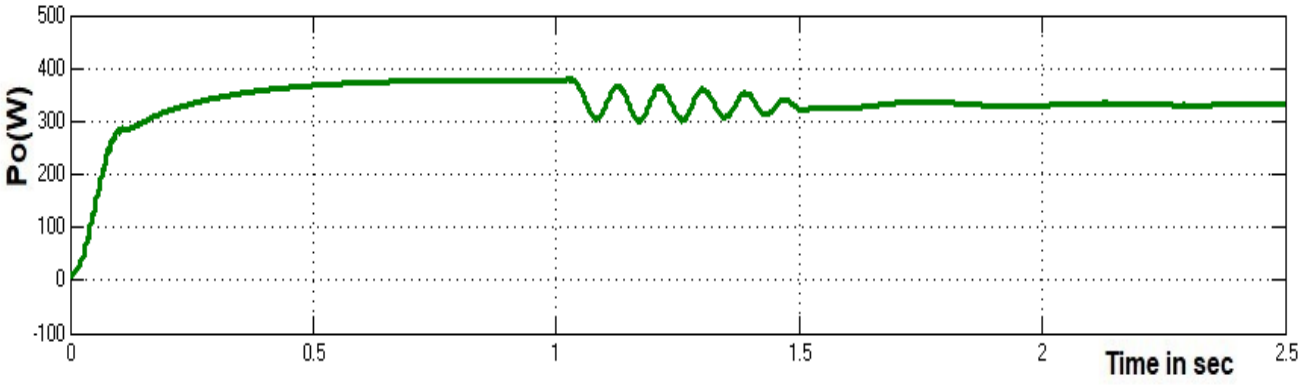

Fig.35. Output power of FC-boost converter with cascaded filter and grid-connected system with closed loop PI controller

The closed PI control is replaced by a Model Predictive (MP) controller, as shown in Fig.36, which takes additional input from the output along with the error. Fig.37 shows the schematic diagram of the MP control circuit. This MP controller receives voltage feedback (Vf) current feedback (If), and reference voltage (Vrf) resulting in providing excitation to the PWM controller, which in turn provides compensatory switching pulses (S1 – S6) for the H bridge inverter and the flying capacitor-based DC-DC converter. The input voltage fed to the DC-DC converter is displayed in Fig.38. The voltage quality across the flying capacitor is improved and maintains a value of 60V, which is shown in Fig.39. However, the oldest and current performance across the RL load remains UN changed with the influence of

Note:- Artificial intelligence tools were used solely for language refinement and formatting support. The technical content, analysis, results, and conclusions were entirely developed by the authors.

switching frequency which shall be visualized shown in Fig.40 and Fig.41. Fig.42 displays the Root Mean Square (RMS) value of the voltage, which is 80V. However, the harmonic performance of voltage and current improved greatly when compared to traditional control, increasing by 1.92% and 1.57%, respectively, as illustrated in Fig.43 and Fig.44and Fig.45 shows the comparable power, which is 360 W.

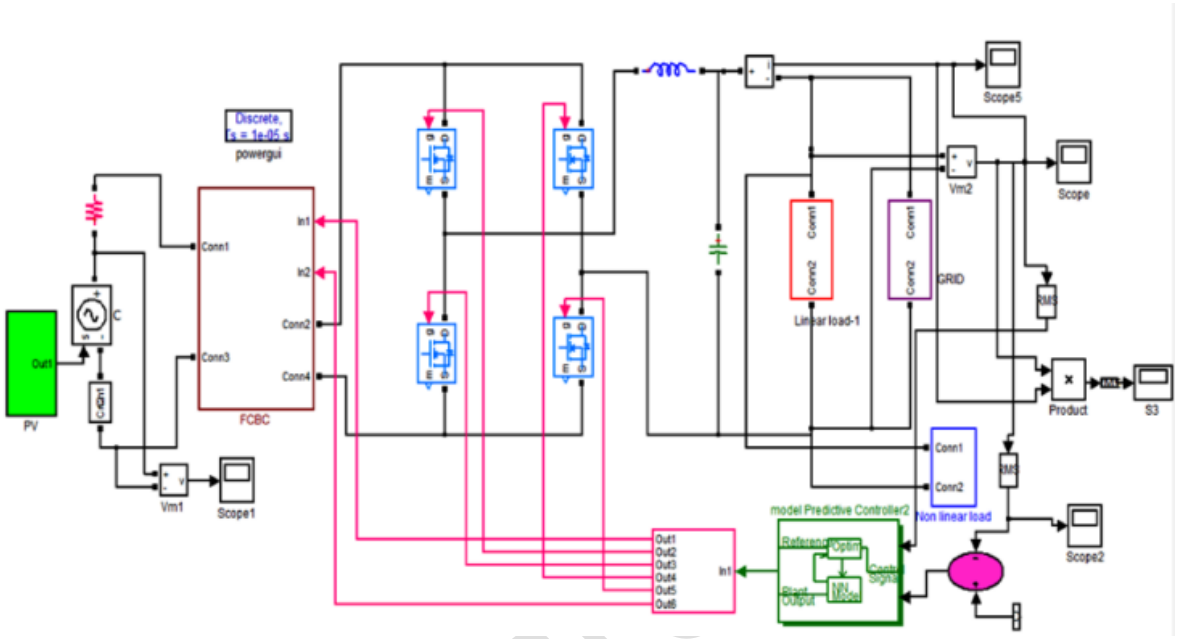

Fig.36. Closed maximum power controller with grid tie inverter and a flying capacitor-based DC-DC converter.

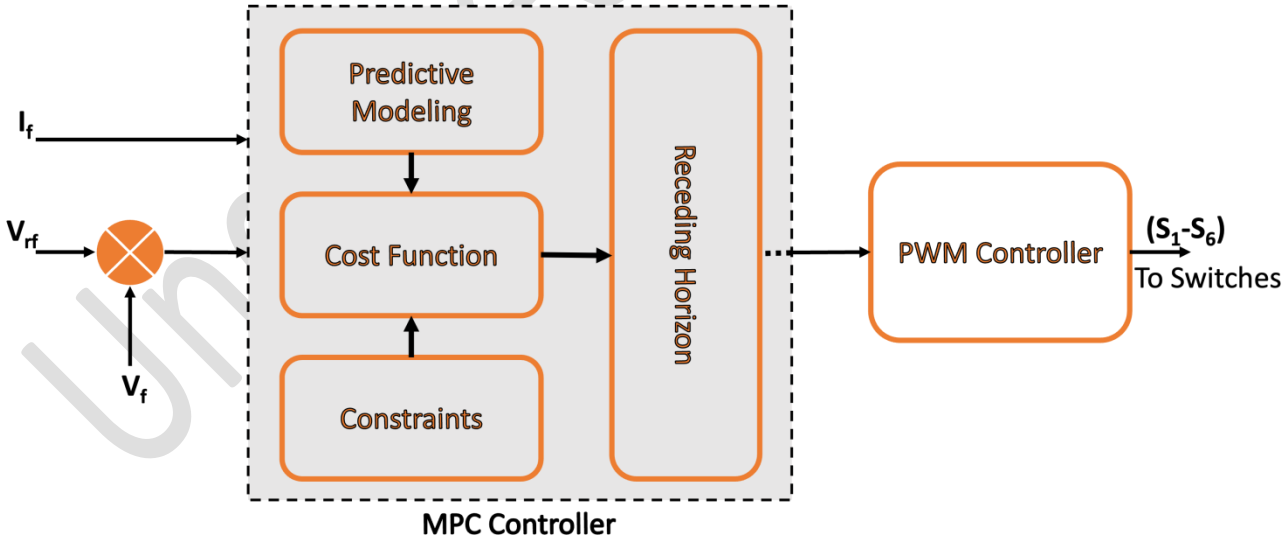

Fig. 37. Schematic of MP control circuit.

Note:- Artificial intelligence tools were used solely for language refinement and formatting support. The technical content, analysis, results, and conclusions were entirely developed by the authors.

10.22060/EEJ.2026.24986.5808

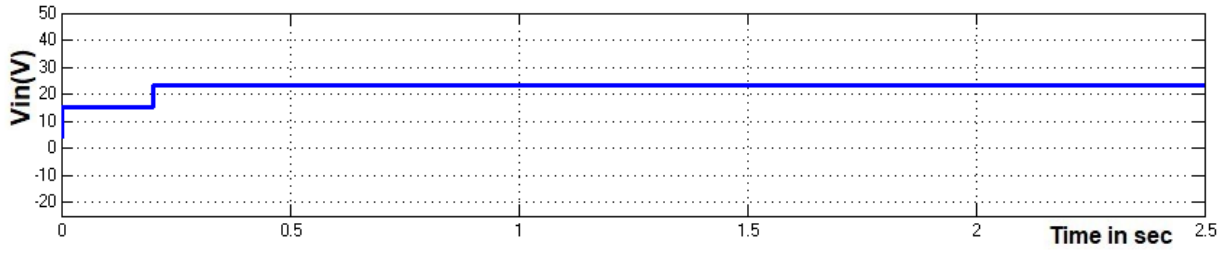

Fig.38. Input voltage in flying capacitor of the boost converter and grid tie inverter with MP controller

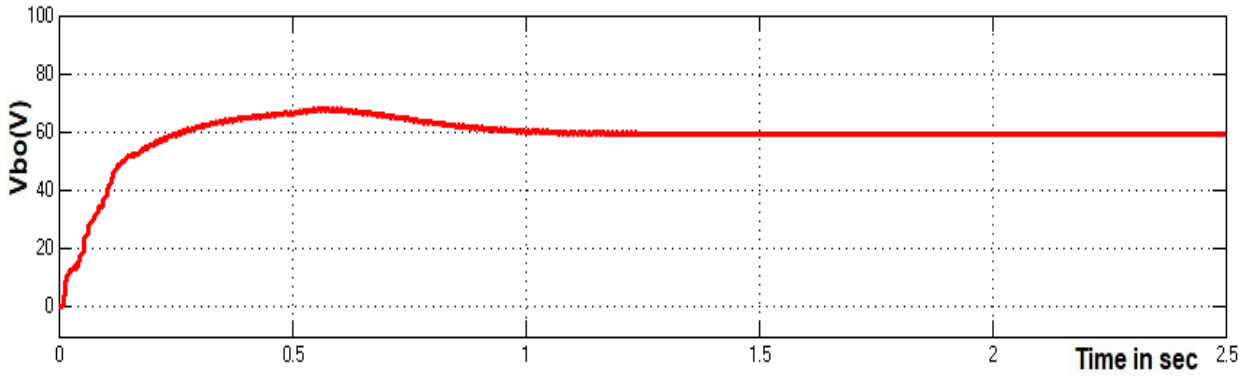

Fig.39. Flying capacitor voltage in boost converter

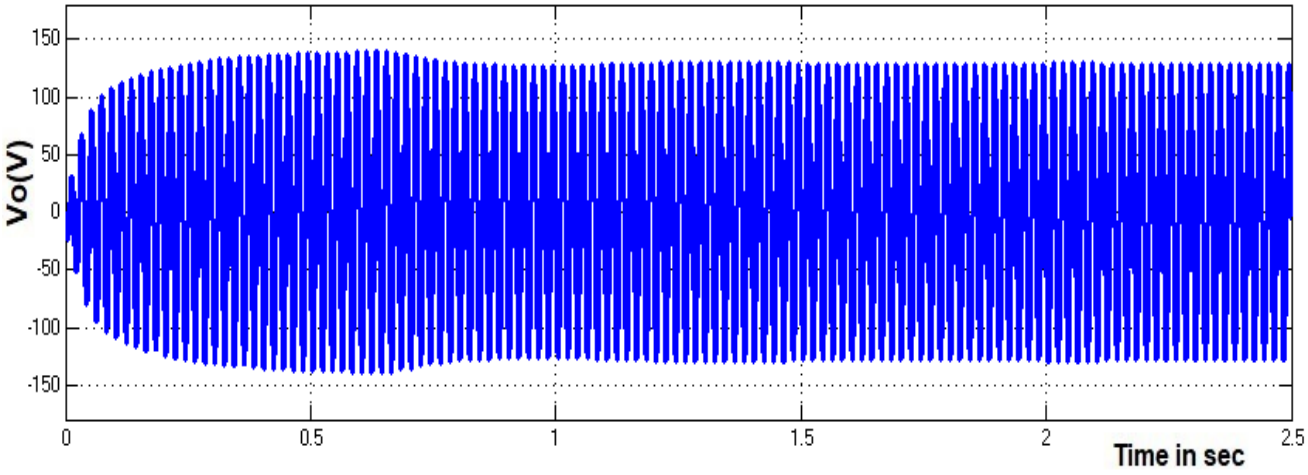

Fig.40. RL load voltage of DC-DC converter and grid tie inverter system with MP controller

Note:- Artificial intelligence tools were used solely for language refinement and formatting support. The technical content, analysis, results, and conclusions were entirely developed by the authors.

10.22060/EEJ.2026.24986.5808

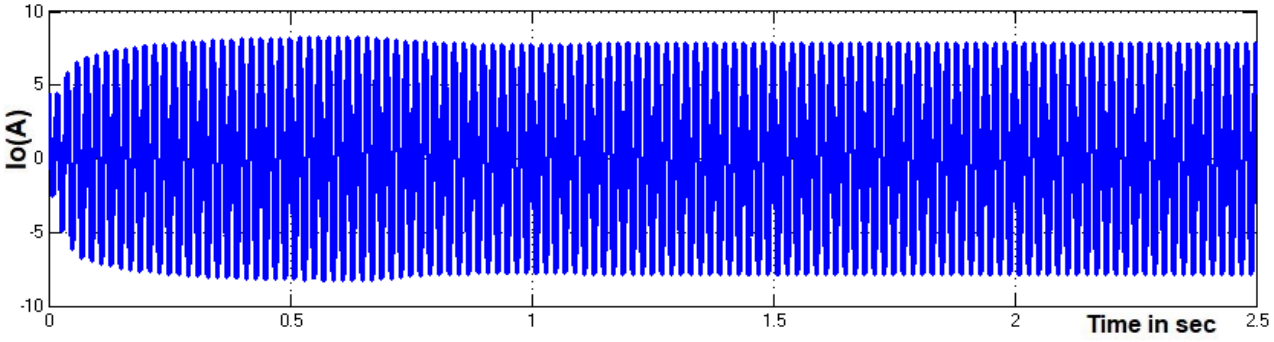

Fig.41. RL load current of the flying capacitor-based converter and grid tie inverter with MP controller

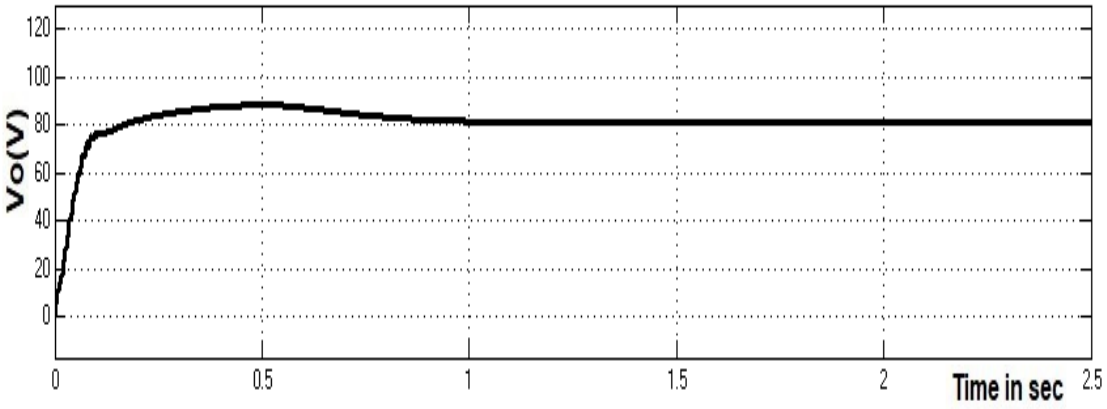

Fig.42. RL load RMS voltage of flying capacitor-based converter and grid tie inverter with MP controller

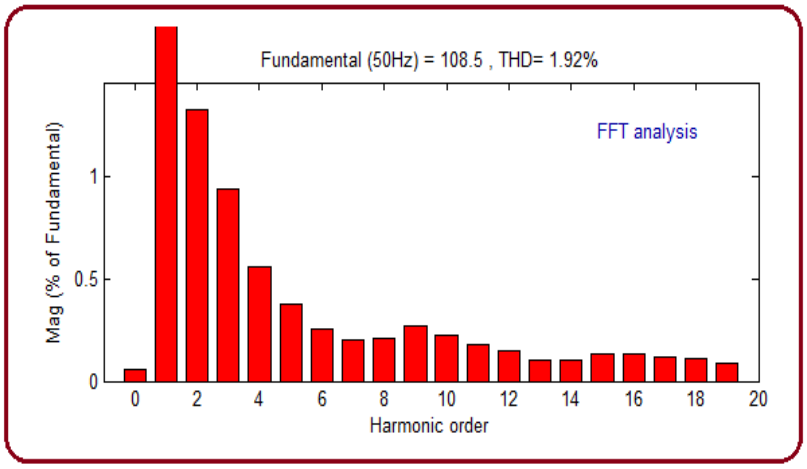

Fig.43. Voltage harmonics

Note:- Artificial intelligence tools were used solely for language refinement and formatting support. The technical content, analysis, results, and conclusions were entirely developed by the authors.

10.22060/EEJ.2026.24986.5808

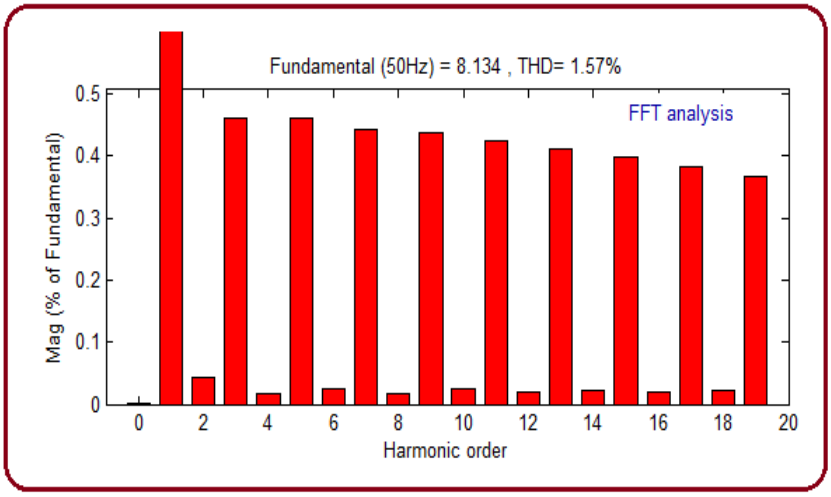

Fig.44. Current harmonics

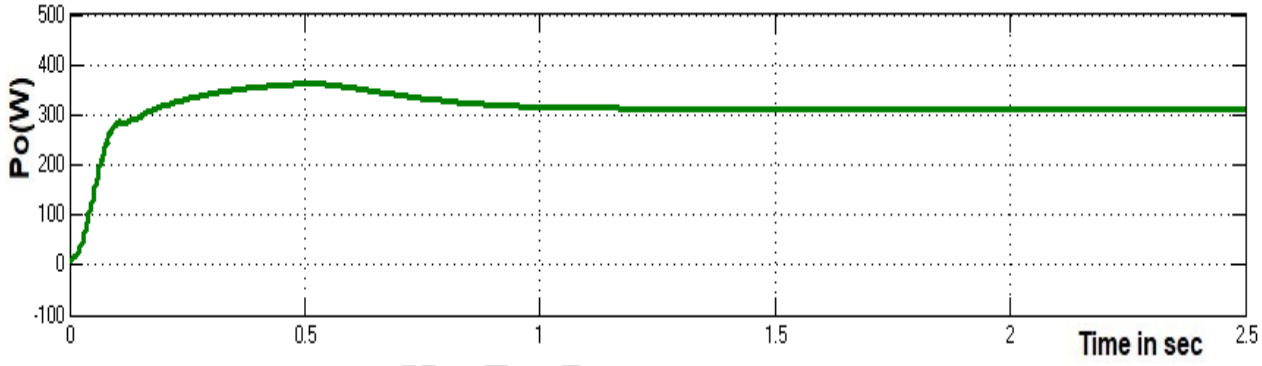

Fig.45. Output power of flying capacitor-based DC-DC Converter and grid tie inverter with MP controller.

The boost converter with flying capacitor and grid-connected inverter inherently exhibits nonlinear behavior due to duty-cycle saturation, switching actions, and load-dependent DC-link dynamics. These nonlinearities become more pronounced during transient operating conditions such as sudden load changes, reference variations, and grid disturbances.

In particular, the relationship between the duty cycle and the DC-link voltage is nonlinear, and conventional PI controllers, which are designed based on linearized operating points, exhibit degraded performance when operating far from their nominal conditions. Switching-induced nonlinearities further introduce time-varying dynamics that cannot be effectively compensated by fixed-gain linear controllers.

Note:- Artificial intelligence tools were used solely for language refinement and formatting support. The technical content, analysis, results, and conclusions were entirely developed by the authors.

MPC Performance Advantage

Although a complete nonlinear state-space formulation is beyond the scope of this work, the proposed model predictive control (MPC) strategy inherently accounts for nonlinear system behavior by utilizing a discrete-time prediction model and real-time feedback of multiple system variables. The MPC incorporates both DC-link voltage and inverter current feedback to predict future system states over a finite horizon and to select the optimal control action that minimizes the cost function.

Unlike PI control, which reacts to instantaneous error, the predictive nature of MPC allows it to anticipate the effects of duty-cycle saturation and switching behavior, thereby improving transient response and steady-state performance under nonlinear operating conditions.

Therefore, the improved performance observed with MPC in terms of reduced settling time, lower overshoot, and decreased harmonic distortion can be attributed to its ability to manage dominant nonlinear characteristics of the converter system more effectively than conventional PI control. The validity of this qualitative justification is supported by the comparative simulation and experimental results presented in this paper.

5. Experimental Results

Fig.46 depicts the experimental findings for a flying capacitor-based DC-DC converter with grid-tied inverter. The hardware comprises a power circuit and a control circuit, respectively. The microcontroller is PIC-16P84A, which is isolated from the power circuit. To reduce EMC/EMI caused by power switching, optical isolation is employed, as are the drivers for the MOSFET with IR2110.

Note:- Artificial intelligence tools were used solely for language refinement and formatting support. The technical content, analysis, results, and conclusions were entirely developed by the authors.

10.22060/EEJ.2026.24986.5808

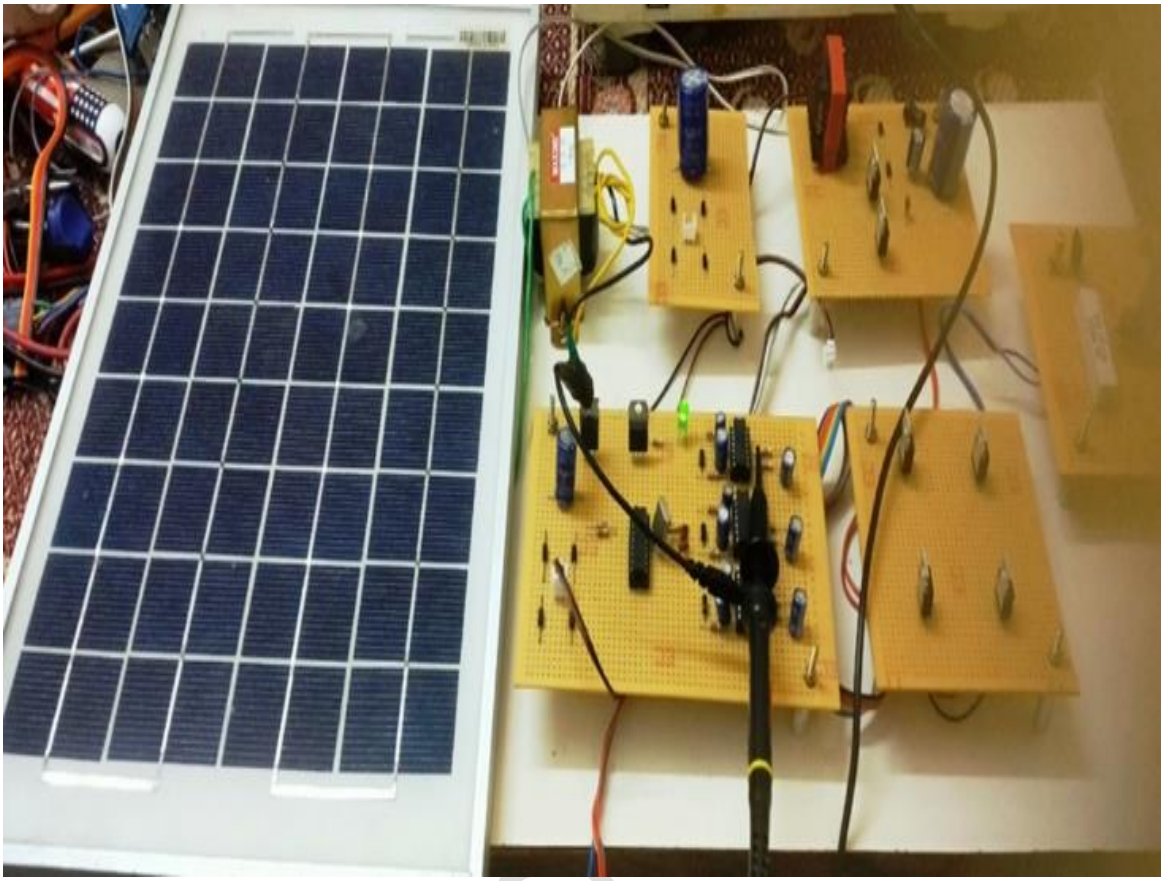

Fig.46. Hardware snapshot of FC-BC and grid-connected inverter system

Table 3. Component specifications of FC-BC integrated to grid connected inverter system

S.No.	Components Name	Values
1.	Capacitor	1000uF,4.7uF, 2.20mF, 3.3pF
2.	Diode	1000V, 3A
3.	Inductance	10uH
4.	MOSFET (IR840)	600V, 8A
5.	Resistor	1kΩ, 100Ω, 22Ω
6.	Potentiometer (Voltage Sensor)	10kΩ
7.	Regulator IC (7812, 7805)	12V,5V
8.	PIC Microcontroller	18 pin, 4V-5.5V
9.	Opto-Coupler (IR2110)	500V/600V
10.	Current Sensor (ACS712)	5A
11.	Printed Circuit Board (PCB)	V105

Note:- Artificial intelligence tools were used solely for language refinement and formatting support. The technical content, analysis, results, and conclusions were entirely developed by the authors.

10.22060/EEJ.2026.24986.5808

The component specifications of the FC-boost converter integrated into grid-connected inverter system is presented in Table 3. In the proposed hardware, the ACS712-based current sensor was utilized to measure current and the potentiometer was utilized as the scaling circuit to measure the output voltage. Generally, the analog pin of the Analog to Digital converter of the PIC microcontroller senses voltage ranges from 0V to 5V. In general, the output voltage produced by the converter/inverter in the closed loop operation will be achieved with feedback and this feedback will be given to the closed loop algorithm which in turn maintains constant output voltage. So, the output voltage produced by the FC-boost converter integrated into grid-connected inverter system is scaled using the potentiometer to match the level of the analog pin of the microcontroller. Furthermore, the current sensor (ACS712) is utilized in this work to sense the current and the output of the current sensor was directly in terms of microcontroller acceptable levels. The input voltage fed to the FC-BC and grid-connected inverter system is shown in Fig.47.

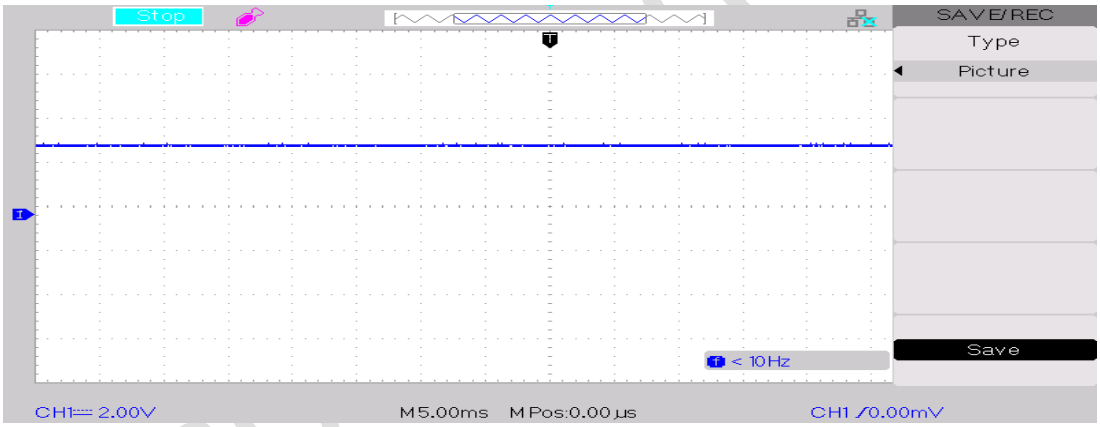

Fig.47. Input voltage of FC-BC and grid-connected inverter system

The switching pulse of the FC-boost converter is shown in Fig.48 and the switching pulses shifted by 180o for grid-connected inverter system is shown in Fig.49.

Note:- Artificial intelligence tools were used solely for language refinement and formatting support. The technical content, analysis, results, and conclusions were entirely developed by the authors.

10.22060/EEJ.2026.24986.5808

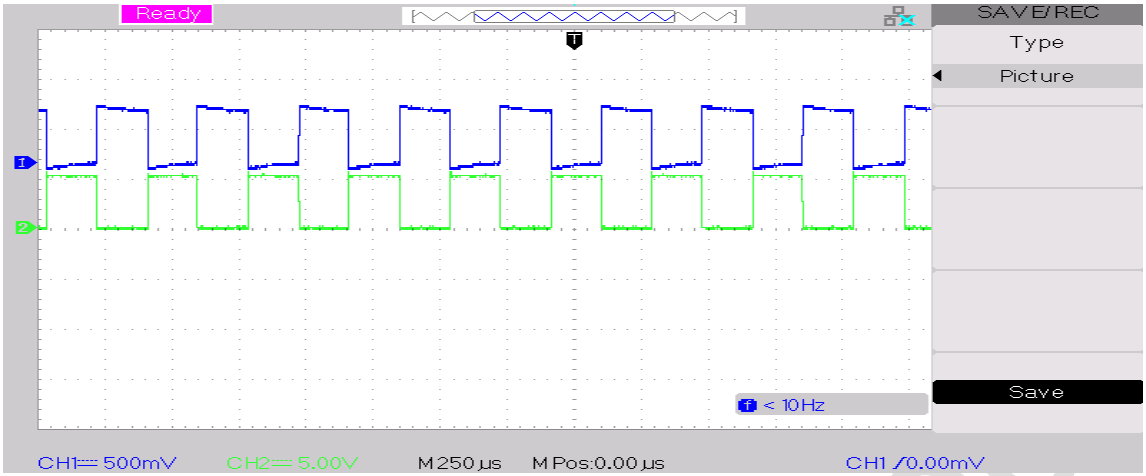

Fig.48. Switching pulse of FC-BC

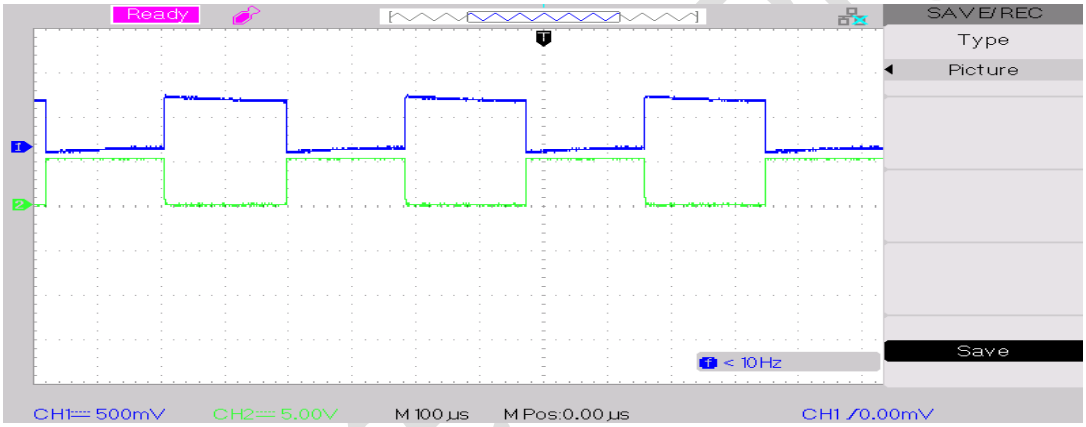

Fig.49. Switching pulses for inverter of FC-BC

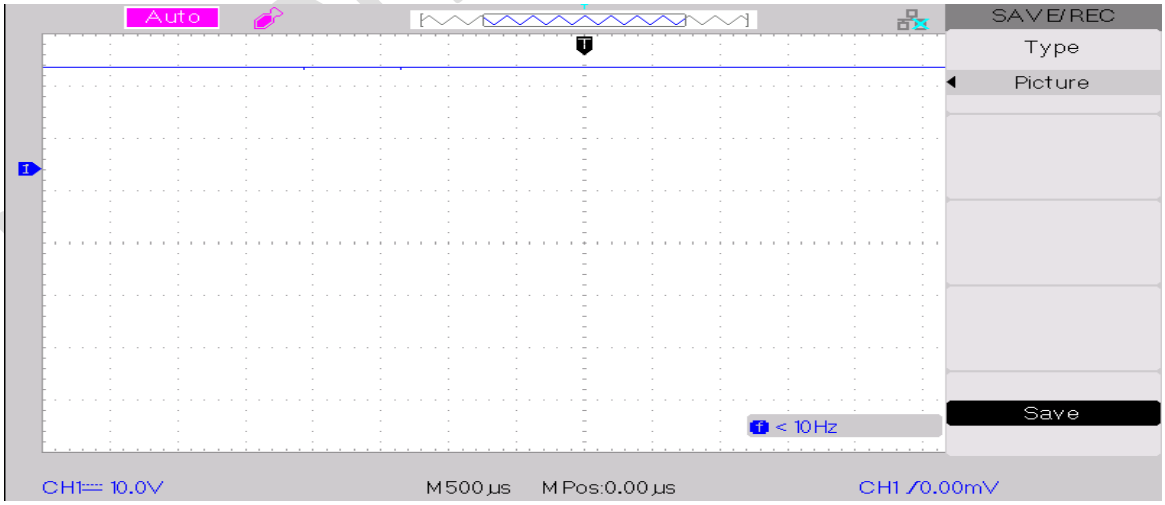

Fig.50. Voltage across FC-boost converter and grid-connected inverter system

Note:- Artificial intelligence tools were used solely for language refinement and formatting support. The technical content, analysis, results, and conclusions were entirely developed by the authors.

10.22060/EEJ.2026.24986.5808

The voltage across FC-BC is shown in Fig. 50 and the voltage across grid-connected inverter shall be visualized in Fig. 51. Furthermore, due to the impact of a single LC filter at the output side, it is observed that the voltage across grid-connected inverter is a distorted sine wave.

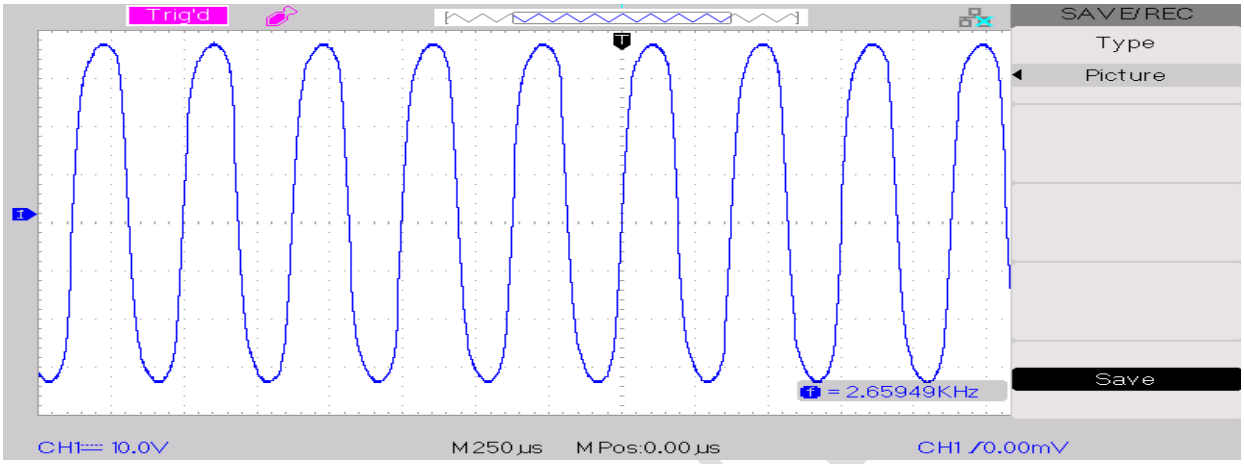

Fig.51. Voltage across the inverter terminals of FC-BC

The two different closed-loop algorithms namely PI and MP were coded inside the PIC microcontroller and the proposed hardware of the FC-boost converter integrated into grid-connected inverter system was subjected to work on both closed-loop methods. Also, the components include a current sensor, voltage sensor, power circuit namely FC-boost converter integrated into grid-connected inverter system, control circuit namely PIC microcontroller, and isolation circuit namely opto-coupler remains the same for both closed loop operations. Additionally, the closed algorithms namely PI and MPC differ. The individual closed-loop algorithm was coded inside the PIC Microcontroller using embedded C language and according to the algorithm, the semiconductor switches were controlled and the output parameters were monitored. Furthermore, the time domain parameters such as rise time (Tr), settling time (Ts), peak time (Tp) and steady-state error (Ess) of FC-boost converter and grid-connected inverter system with closed loop PI controller and MP controller are compared and is presented in Table 4.

Table 4. Improvement in voltage and current harmonics controller

Controller	Voltage THD (%)	Current THD (%)
PI	2.41	2.32
MPC	1.92	1.57

Note:- Artificial intelligence tools were used solely for language refinement and formatting support. The technical content, analysis, results, and conclusions were entirely developed by the authors.

From Table 4, it is seen that the time domain parameters of the FC-boost converter and grid-connected inverter system with closed loop MP controller are superior to the FC-boost converter and grid-connected inverter system with closed loop PI controller. Also, the Tr, Ts, Tp and Ess values of the FC-boost converter and grid-connected inverter system with two different closed-loop namely PI and MP controller are presented in Table 4.

In a closed-loop system, the fundamental concern is the system's dynamic performance, and harmonics play a significant part in improving power quality. In the proposed controller, the voltage and current harmonics improved significantly, as presented in Table 4. For dynamic performance, the various parameters such as Tr, Ts, Tp and Ess are improved significantly, as presented in Table 5.

Table 5. Improvement in dynamic performance with proposed FC-boost converter and grid-connected inverter system with closed loop controllers

Controller	Tr (Sec)	Ts (Sec)	Tp (Sec)	Ess (Sec)
PI	0.62	1.52	0.88	1.69
MPC	0.40	0.96	0.54	0.73

The proposed controller helps to improve power quality and system stability when compared to classical PI regulators.

Closed-Loop Stability Considerations

The closed-loop stability of the proposed flying capacitor boost converter integrated with a grid-tied inverter is discussed qualitatively in this section. The overall system is inherently nonlinear due to switching actions, duty-cycle constraints, and load-dependent dynamics. Nevertheless, bounded-input bounded-output (BIBO) stability is ensured through constrained duty-cycle regulation and energy balancing across the DC-link capacitors.

These results suggest that the predictive nature of MPC, combined with multi-variable feedback, enhances the system’s tolerance to parameter variations and load disturbances commonly encountered in smart grid applications.

6. Conclusion

An existing single-stage DC-DC boost converter with a grid tie inverter system and the proposed boost converter with a flying capacitor grid tie inverter system were simulated and compared. Further, the

Note:- Artificial intelligence tools were used solely for language refinement and formatting support. The technical content, analysis, results, and conclusions were entirely developed by the authors.

proposed two different converter topologies namely boost converter with flying capacitor integrated to grid tie inverter system with C-filter and Cascaded-filter were simulated. Also, the voltage and current harmonics of two different controllers namely PI and MPC were analyzed. The proposed circuit converter with flying capacitor cascaded filter integrated into a grid tie inverter system with closed loop PI controller and MP controller was simulated. Results demonstrate that the boost converter with flying capacitor Cascaded-Filter and grid tie inverter system has a reduced ripple voltage of 0.5V which is superior than the flying capacitor boost converter with C-Filter that exhibits a ripple voltage of 1.2V. Furthermore, it is demonstrated that the output current THD of the flying capacitor boost converter with a cascaded filter is 4.79%. Also, it is observed that the boost converter with flying capacitor cascaded filter integrated to grid tie inverter system with closed-loop MP controller has a rise time of 0.40s, the peak time of 0.54s, settling time of 0.96s and steady-state error voltage of 0.73V which is better than flying capacitor boost converter with a cascaded filter integrated to grid-connected inverter system with closed loop PI controller. The voltage THD and current THD of the flying capacitor boost converter with cascaded filter and grid-connected inverter system with closed-loop MP controller is 1.92% and 1.57% respectively. From the results, it is demonstrated that the flying capacitor boost converter with cascaded filter and grid-connected inverter system with closed-loop MP controller is superior when compared to the same topology with PI controller. However, the MP controller is very complex to compute/implement in real-time, it can be avoided using cost-effective advanced Digital Signal Processors (DSP).

Declaration

Conflict of Interest

The corresponding author declares no conflict of interest on behalf of all authors.

Availability of Data and Materials:

The data sets generated during and/or analyzed during the current study are available from the corresponding author on reasonable request.

Funding:

Not applicable.

References

1. R. V. Babu, P. M. Kumar and G.S.Rao, "Design & modeling of fuel cell powered quadratic Boost converter based multi-level inverter", 2017 Innovations in Power and Advanced Computing Technologies (i-PACT), Vellore, 2017, pp.1-6.

Note:- Artificial intelligence tools were used solely for language refinement and formatting support. The technical content, analysis, results, and conclusions were entirely developed by the authors.

2. Almeida, P. S., Braga, H. A., Dalla Costa, M. A., & Alonso, J. M. (2014). Offline soft-switched LED driver based on an integrated bridgeless boost–asymmetrical half-bridge converter. IEEE Transactions on Industry Applications, 51(1), 761-769.
3. M.A.AlSaffar, E.H.Ismail and A.J.Sabzali, "High efficiency quadratic boost converter", 2012 -Twenty Seventh Annual IEEE Applied Power Electronics Conference and Exposition (APEC), Orlando, FL, -2012, pp-1245-1252.
4. J. D. Navamani, J. M. Raj, K. Vijayakumar and A. Lavanya, "Analysis of modified quadratic DC-DC boost converter," 2017 International Conference on Inventive Systems & Control (ICISC), Coimbatore, 2017, pp. 1-5.
5. Ping Yang, Jianping Xu, Guohua Zhou and Shiyu Zhang, "A-new-quadratic-boost converter-with-high-voltage-step-up-ratio-and-reduced-voltage-stress," Proceedings of the 7th International P.E & Motio Control Conference, Harbin, 2012, pp. 1164-1168.
6. S. Zhang, J. Xu and P. Yang, "A single switch high gain quadratic boost converter based on voltage lift technique", 2012 10th International Power & Energy Conference (IPEC), Ho Chi Minh City, 2012, pp. 71-75
7. Kuo, J.K., "An integrated simulation model for PEM fuel cell power systems with a buck DC –DC converter", International Journal of Hydrogen Energy, vol.36, no.18, pp.11846-11855, September 2011.
8. T. R. Choudhury and B. Nayak, "Comparison & analysis of cascaded & Quadratic Boost Converter," 2015 IEEE Power, Communication & Information Technology Conference (PCITC), Bhubaneswar, 2015, pp. 78-83.
9. V.Vijayakumar, R.Divya, and A.Vivek, “Sliding mode controlled quadratic boost converter”, in IEEE International Conference on Computation of Power, Energy, Information and Communication, 2014, pp. 189-193.
10. J. Choi, H. S. Han, and K. Lee, “A current-sourced LED driver compatible with fluorescent lamp ballasts", IEEE Trans. Power Electron., vol. 30, no. 8, pp. 4455_4466, Aug. 2015.
11. P. S. Almeida, H. A. C. Braga, M. A. D. Costa, and J. M. Alonso, “Offline soft-switched LED driver based on an integrated bridgeless boost asymmetrical half-bridge converter", IEEE Trans. Ind. Appl., vol. 51, no. 1, pp. 761_769, Jan./Feb. 2015.
12. X. Ruan, B. Wang, K. Yao, and S. Wang, “Optimum injected current harmonics to minimize peak-to-average ratio of LED current for electrolytic capacitor-less AC_DC drivers” IEEE Trans. Power Electron., vol. 26, no. 7, pp. 1820_1825, Jul. 2011.
13. Q. Luo, S. Zhi, C. Zou, B. Zhao, and L. Zhou, “Analysis and design of a multi-channel constant current light-emitting diode driver based on high frequency AC bus", IET Power Electron., vol. 6, no. 9, pp. 1803_1811, Nov. 2013.
14. M. Arias, D. G. Lamar, J. Sebastian, D. Balocco, and A. A. Diallo, “High-efficiency LED driver without electrolytic capacitor for street lighting”, IEEE Trans. Ind. Appl., vol. 49, no. 1, pp. 127_137, Jan./Feb. 2013.
15. X.Wu, C. Hu, J. Zhang, and Z. Qian, “Analysis and design considerations of LLCC resonant multioutput DC/DC LED driver with charge balancing and exchanging of secondary series resonant capacitors", IEEE Trans. Power Electron., vol. 30, no. 2, pp. 780_789, Feb. 2015.
16. Aourir, M., Abouloifa, A., Aouadi, C., Otmani, F. E., Lachkar, I., Noussi, K., & Katir, H. (2022). Hybrid Control of Flying Capacitor Converter Based Shunt Active Power Filter for Photovoltaic Systems Interconnection. In IFAC-PapersOnLine (Vol. 55, Issue 12, pp. 49–54). Elsevier BV. https://doi.org/10.1016/j.ifacol.2022.07.287
17. X. Jiang and M. L. Doumbia, "Comparative Study of Grid-Connected Multilevel Inverters for High Power Phtovoltaic Systems," 2019 IEEE 7th International Conference on Smart Energy Grid Engineering (SEGE), Oshawa, ON, Canada, 2019, pp. 184-190, doi: 10.1109/SEGE.2019.8859784.

Note:- Artificial intelligence tools were used solely for language refinement and formatting support. The technical content, analysis, results, and conclusions were entirely developed by the authors.

18. Taghzaoui, C., Abouloifa, A., Tighazouane, B., Aicha, E., Lachkar, I., Mchaouar, Y., & Giri, F. (2022). Advanced Control of Single-Phase Shunt Active Power Filter Based on Flying Capacitor Multicell Converter. In IFAC-PapersOnLine (Vol. 55, Issue 12, pp. 55–60). Elsevier BV. https://doi.org/10.1016/j.ifacol.2022.07.288
19. Oghorada, O. J. K., Zhang, L., Esan, B. A., & Dickson, E. (2019). Carrier-based sinusoidal pulse-width modulation techniques for flying capacitor modular multi-level cascaded converter. In Heliyon (Vol. 5, Issue 12, p. e03022). Elsevier BV. https://doi.org/10.1016/j.heliyon.2019.e03022
20. C. Zhang, M. Xu, W. Wang, X. Meng and Z. Kan, "A High-gain Floating-Interleaved Three-level Boost Converter," 2019 4th International Conference on Intelligent Green Building and Smart Grid (IGBSG), Hubei, China, 2019, pp. 126-131, doi: 10.1109/IGBSG.2019.8886224.
21. S. Rahimpour, O. Matiushkin, N. V. Kurdkandi, M. Najafzadeh, O. Husev and D. Vinnikov, "Model Predictive Control of A Single-Stage Flying Inductor Based Buck-Boost Grid-Connected Common-Ground Inverter," 2021 IEEE 62nd International Scientific Conference on Power and Electrical Engineering of Riga Technical University (RTUCON), Riga, Latvia, 2021, pp. 1-6, doi: 10.1109/RTUCON53541.2021.9711711.
22. Eguchi, K., Abe, H., Ishibashi, T., & Asadi, F. (2020). The development of a step-down switched-capacitor inverter without flying capacitors and full-bridge circuits. In Energy Reports (Vol. 6, pp. 257–262). Elsevier BV. https://doi.org/10.1016/j.egyr.2019.11.071
23. Hemici, K., Zegaoui, A., Bokhtache, A. A., Mahmoudi, M. O., & Aillerie, M. (2015). Three-Phases Flying-Capacitor Multilevel Inverter with Proportional Natural PWM Control. In Energy Procedia (Vol. 74, pp. 1061–1070). Elsevier BV. https://doi.org/10.1016/j.egypro.2015.07.744
24. Laamiri, S., Ghanes, M., Amet, L., & Santomenna, G. (2017). Direct Control Strategy for a Three Phase Eight-Level Flying-Capacitor Inverter. In IFAC-PapersOnLine (Vol. 50, Issue 1, pp. 15786–15791). Elsevier BV. https://doi.org/10.1016/j.ifacol.2017.08.2315
25. Z. Ye, Y. Lei, Z. Liao and R. C. N. Pilawa-Podgurski, "Investigation of Capacitor Voltage Balancing in Practical Implementations of Flying Capacitor Multilevel Converters," in IEEE Transactions on Power Electronics, vol. 37, no. 3, pp. 2921-2935, March 2022, doi: 10.1109/TPEL.2021.3119409.
26. X. Zhao, Y. Zhang and Q. Guan, "A Balancing Control Method for Flying Capacitors in Five-Level Buck/Boost Converter with Synchronous Phase Shifting Decoupling," 2021 IEEE 1st International Power Electronics and Application Symposium (PEAS), 2021, pp. 1-6, doi: 10.1109/PEAS53589.2021.9628490.

Note:- Artificial intelligence tools were used solely for language refinement and formatting support. The technical content, analysis, results, and conclusions were entirely developed by the authors.